

Journal Pre-proofs

Discovery of 5-Naphthylidene-2,4-thiazolidinedione derivatives as selective HDAC8 inhibitors and evaluation of their cytotoxic effects in leukemic cell lines

Kalpna Tilekar, Neha Upadhyay, Niklas Jansch, Markus Schweipert, Piotr Mrowka, F.J. Meyer-Almes, C.S. Ramaa

PII: S0045-2068(19)31633-5
DOI: <https://doi.org/10.1016/j.bioorg.2019.103522>
Reference: YBIOO 103522

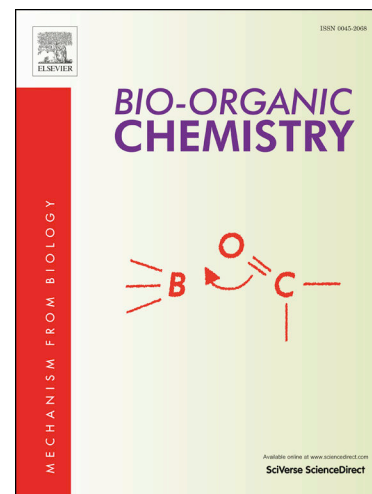
To appear in: *Bioorganic Chemistry*

Received Date: 2 October 2019
Revised Date: 14 December 2019
Accepted Date: 17 December 2019

Please cite this article as: K. Tilekar, N. Upadhyay, N. Jansch, M. Schweipert, P. Mrowka, F.J. Meyer-Almes, C.S. Ramaa, Discovery of 5-Naphthylidene-2,4-thiazolidinedione derivatives as selective HDAC8 inhibitors and evaluation of their cytotoxic effects in leukemic cell lines, *Bioorganic Chemistry* (2019), doi: <https://doi.org/10.1016/j.bioorg.2019.103522>

This is a PDF file of an article that has undergone enhancements after acceptance, such as the addition of a cover page and metadata, and formatting for readability, but it is not yet the definitive version of record. This version will undergo additional copyediting, typesetting and review before it is published in its final form, but we are providing this version to give early visibility of the article. Please note that, during the production process, errors may be discovered which could affect the content, and all legal disclaimers that apply to the journal pertain.

© 2019 Published by Elsevier Inc.



Discovery of 5-Naphthylidene-2,4-thiazolidinedione derivatives as selective HDAC8 inhibitors and evaluation of their cytotoxic effects in leukemic cell lines.

Kalpana Tilekar^a, Neha Upadhyay^a, Niklas Jansch^c, Markus Schweipert^c, Piotr Mrowka^b, F. J. Meyer-Almes^{c*}, C. S. Ramaa^{a*},

^aDepartment of Pharmaceutical Chemistry, Bharati Vidyapeeth's college of Pharmacy, Navi Mumbai, Maharashtra, India; ^bDepartment of Biophysics and Human Physiology, Medical University of Warsaw, Chalubinskiego, Warsaw, Poland; ^cDepartment of Chemical Engineering and Biotechnology, University of Applied Sciences Darmstadt, Germany.

*Corresponding authors.

1. C S Ramaa

E-mail address: sinharamaa@yahoo.in

Tel.: +91 22 27572131/1122; Fax: +91 22 27574515.

2. Franz-Josef Meyer-Almes

Email : franz-josef.meyer-almes@h-da.de

Phone: +49 6151168406; Fax : +49 6151168404

Abstract

Histone deacetylases (HDACs) are being explored as a therapeutic target for interventions in different types of cancer. HDAC8 is a class I HDAC that is implicated as a therapeutic target in various indication areas, including different types of cancer and particularly childhood neuroblastoma. Most previously described HDAC8-selective inhibitors contain a hydroxamate function as zinc binding group (ZBG) to confer potency. However, hydroxamate class HDAC inhibitors have raised increasing concerns about their mutagenic character. Therefore, non-hydroxamate based inhibitors could prove to be safer than hydroxamates. In the present work, a series of novel 5-naphthylidene-2,4-thiazolidinedione was designed and evaluated as potential antiproliferative agents targeting selectively HDAC8 enzyme. Eleven novel derivatives were synthesized, purified and characterized by spectroscopic techniques. Compounds **3k** and **3h** was found to be most potent selective inhibitors of HDAC8 with IC₅₀ values of 2.7 μM and 6.3 μM respectively. **3a** to **3i** was found to be most cytotoxic in leukemic cell lines. **3a** and **3h** both were found to induce apoptosis and cause cell cycle arrest in G2/M phase.

Keywords

HDAC8; Antiproliferative; Thiazolidinedione (TZD); Naphthalene; Leukemia; Cytotoxicity.

1. Introduction

Epigenetic abnormalities are hallmarks of carcinogenesis and cancer progression [1]. Histone deacetylases (HDACs) are major regulators for chromatin remodeling and epigenetics via

deacetylation of acetylated lysine residues of histone and non-histone proteins. Therefore, HDACs have been considered to be relevant targets for therapeutic intervention in different types of cancer. Meanwhile, HDACs have become established targets, predominantly for cutaneous T-cell lymphoma and multiple myeloma [2, 3]. At this time five HDAC inhibitors have been approved world wide (vorinostat, romidepsin, panobinostat, belinostat, and chidamide), which are more or less nonselective.

HDACs belong to the major enzyme family of lysine deacetylases, which are divided into 4 classes: Classes I, II, subdivided into IIa and IIb, and IV contain a catalytic zinc ion within the active site and are referred to as HDACs in the narrower sense. Class III deacetylases are named sirtuins and their activity depends on NAD⁺. In human cells 11 HDACs and 7 sirtuins are expressed.

Class I member HDAC8 has been considered as promising target for childhood neuroblastoma, T-cell lymphoma [4, 5] and connected to several other types of cancer [6, 7]. The structure activity relationship analysis of HDAC8 inhibitors containing the widely used hydroxamate group as ZBG revealed a fish-like structural arrangement for HDAC inhibitors with hydrophobic aromatic cap function as head to recognize surface regions and a tail comprising the ZBG[8]. Cap group and ZBG are connected by a mostly hydrophobic linker. The characteristic malleability of the binding pocket of HDAC8 enabled the development of isoenzyme selective hydroxamate inhibitors containing hydroxamate group as zinc binding group (ZBG) such as PCI-34051 [5].

In order to analyze the molecular determinants for selective inhibition of HDAC8 diverse classes of HDAC8 inhibitors with different ZBGs were analyzed by using structure activity relationships and Bayesian classification approaches [9]. Benzamides show selectivity for class I HDACs 1, 2 and 3 but are dramatically less active on HDAC8 that is also a member of class I, whereas electrophilic ketones have been developed which inhibit preferably class IIa HDACs and HDAC8 demonstrating that the binding pocket of HDAC8 shares features of class II as well as class I HDACs. These analyses revealed that hydroxamates or carboxylates would be the most beneficial ZBGs. Moreover, so called linkerless compounds with bulky head groups also show selectivity for HDAC8. Many analogs with cyclic linkers attached to hydroxamate group found to exhibit HDAC8 selectivity (Fig. 1).

However, hydroxamate groups are inherently unselective and could potentially interfere with other enzymes containing divalent cations or metal homeostasis. Moreover, some suspicion about the potentially mutagenic character of compounds with hydroxamate groups has been raised, which is particularly critical for long term treatments [10]. Therefore, HDAC inhibitors without hydroxamate as ZBG promise to be more beneficial in terms of selectivity and toxicity. A wide number of non-hydroxamate structures with carboxylates, electrophilic ketones, benzamides, and cyclic peptides as zinc binding groups (ZBGs) have been reported earlier and shown to inhibit the activity of different subtypes of HDACs [11-14]. But only a few non-hydroxamate compounds have been described as isozyme selective inhibitor of HDAC8, such as amino acid derivatives that demonstrate isoform selectivity via access to the internal acetate release channel of the enzyme[15], azetidinone (β lactams) with N-thiomethyl group [16], metabolites of organoselenium compounds such as methylselenocysteine (MSC) and selenomethionine(SM) [17], a dihydroimidazole-thiones [18] or most recently pyrimido [1,3]benzothiazin-derivatives [19-20].

In the light of the drawbacks of the hydroxamate ZBG regarding potential mutagenicity, poor pharmacokinetics and bioavailability, a broad variety of alternative ZBGs were explored and the structure-activity relationship of corresponding classes of inhibitors analyzed [21]. However without any doubts, there is still urgent need for new pharmacophores that do not contain hydroxamate groups and can be developed to selective and potent HDAC8 inhibitors.

2. Results and discussion

2.1 Designing of the molecules.

We designed our novel series of naphthylidene TZDs based on proposed structural backbone of HDAC8 inhibitors (Fig. 2), with the following considerations:

LINKER- Attempts towards the discovery of hydroxamic acid derivatives with HDAC8 selectivity, that fit into the unique sub-pocket of HDAC8, have been found to contain cyclic linkers such as indole-**1,6** [23-24], benzo-triazole- **2** [25-27], benzyl- **3,4** [28], tetrahydro-isoquinoline- **5** [29-31] (Fig. 1). It has been proven that naphthalene hydroxamate analogs, **6** possess higher HDAC-8 selectivity over HDAC1 and HDAC6 [32-33] (Fig. 1), which gave us impetus to develop HDAC inhibitors with cyclic linker, naphthalene.

SPACER- We introduced -CH=CH- as a spacer between linker and ZBG, as it was hypothesized that selective inhibition of HDAC8 may be implicated by a beneficial balance between the chemical structure and conformational flexibility of those inhibitors. Compound 7 (Fig. 2) and similar molecules with -CH=CH-, unsaturated spacer have been reported to show promising HDAC8 inhibitory activities and some of them are currently under clinical investigations [34]. Moreover, naphthalene hydroxamate analogs with unsaturated linker spacer showed higher HDAC-8 selectivity over HDAC-1 and -6 [32].

CAP- Our molecules contain phenyl acetamide in cap portion, as in SAHA and α -cetomide. HDAC8 inhibitors with phenyl acetamide group in cap, have also been reported, however selectivity has not been related to this particular functionality [16]

ZBG- In search of non-hydroxamate HDAC inhibitors, we have earlier reported 2,4-thiazolidenedione [35] as ZBG, compound 9, (Fig. 2), which we have retained in this series of compounds.

Further structural analyses revealed that HDAC8-selective inhibitors show an L-shaped structure, to enable interactions with residues of an HDAC8-specific side pocket [36]. Hou et al [37] virtually screened some HDAC8 inhibitors and validated ZBG-based pharmacophore models (Fig. 2). Finally, we arranged all the fractions with the naphthalene linker being ortho substituted with the purpose of deriving an L-shaped structure, conforming to Hou's pharmacophoric model (Fig. 2).

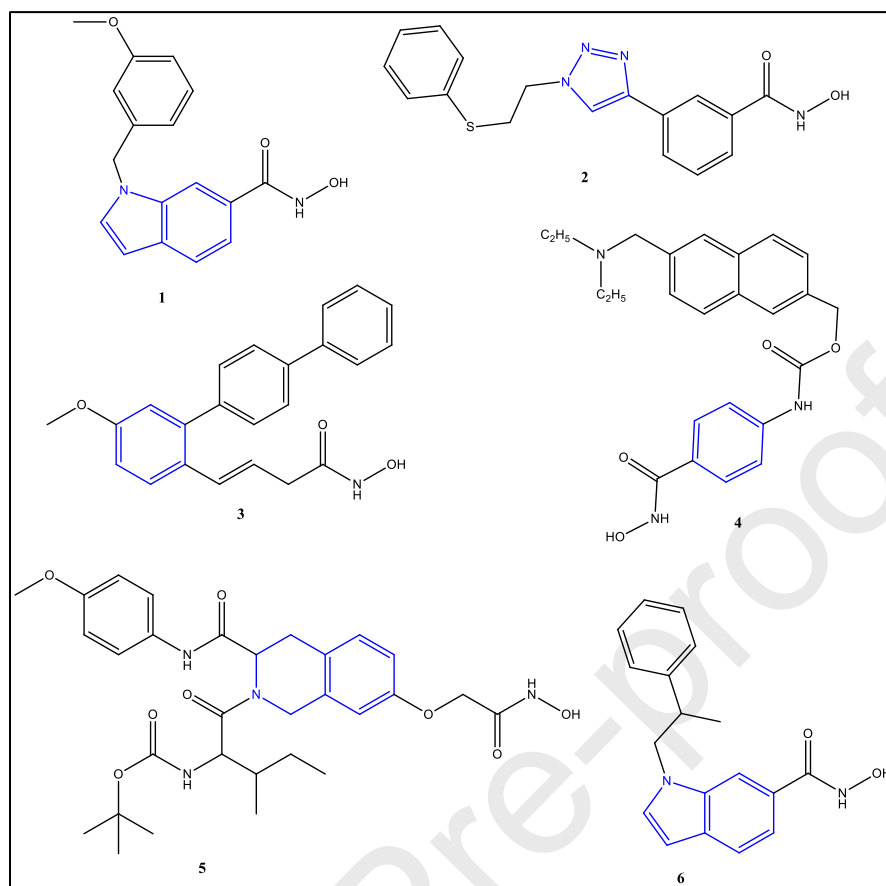


Fig.1. Reported HDAC8 inhibitors with hydroxamic acid as ZBG.

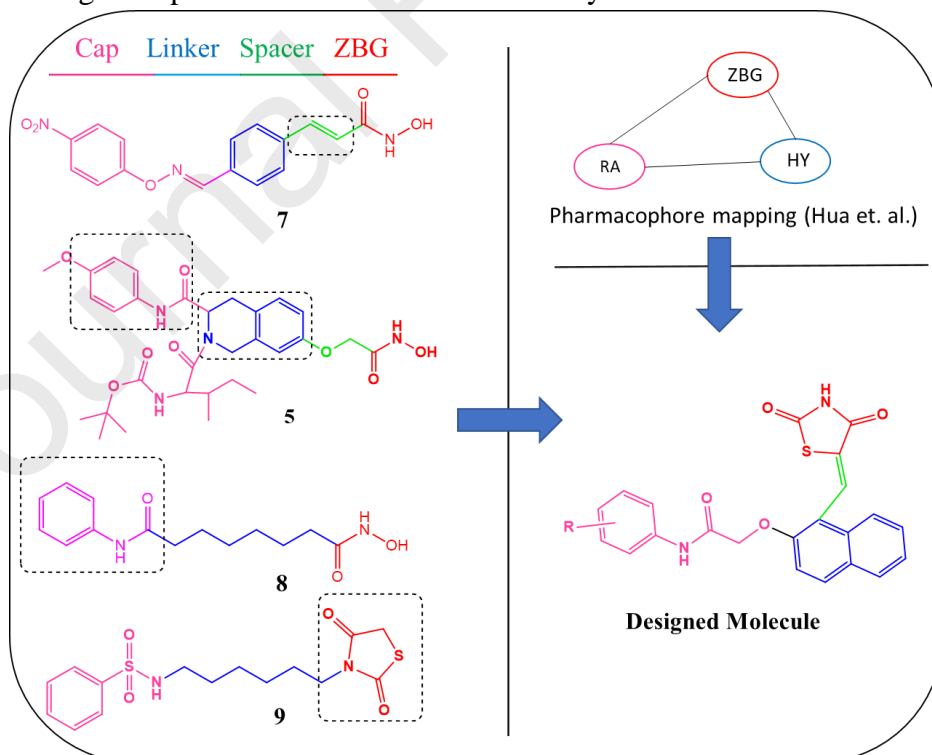


Fig.2. Designing considerations of novel series targeting HDAC8.

2.2 Chemistry

The synthetic route of the compounds is outlined in Scheme 1. A new class of 5-Naphthylidene-2,4-thiazolidinedione derivatives, **3a-3k** (Scheme 1), were synthesized from the condensation of synthetic intermediates **1a** with **2a-2k**. **1a** was synthesized from **1** and **2** (Scheme 1) by Knoevenagel condensation as described previously [38], with slight modifications, in which the product formed was removed intermediately. The product was obtained in good yield of 85% and was yellow crystalline needles. The ¹H NMR spectra of **1a** displayed 3 singlets at 12.59, 10.21 and 8.04 ppm representing the protons of -NH (broad singlet), -OH and benzyldiene double bond (Ph-CH=C) respectively, confirming the formation of **1a**. Discussion about the chemistry **2a-2k** has been described in our previously published work [38-39].

In the IR spectra of **3a-3k** the band for CO-NH-CO and C=O were seen in the region 3400-3300 cm⁻¹ and 1700-1650 cm⁻¹ respectively. In the ¹H NMR spectra, presence of singlet between 4.1-4.5 ppm, provides evidence for formation of -CH₂-O- linkage in final compounds, **3a-3k**. The singlet at 7.9-8.1 ppm is characteristic of benzyldiene proton which confirms that the molecules are in Z-configuration, as described by Momose et al [40]. Additional spectral characteristics were conformed by ¹³C NMR and Mass spectroscopy and are presented in experimental section.

2.3 In vitro HDAC screening

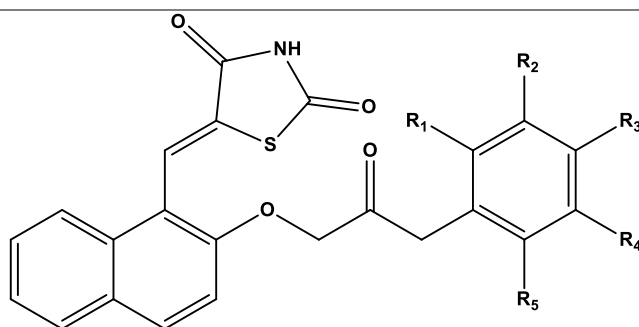
2.3.1 HDAC enzyme inhibition Assay

To assess selectivity, the synthesized derivatives were screened against a panel of human HDAC isoenzymes using procedures described in method section. Interestingly 6 out of 11 compounds displayed potent inhibition of HDAC8 compared to the other HDAC isoenzymes (Table 1, Fig. 3). The derivatives that exhibited maximum selectivity with IC₅₀ values less than 15 μM were, 4-nitro(**3k**), 4-bromo (**3i**), 3-trifluoromethyl (**3j**), 2-fluoro-4-bromo (**3h**) and 2-bromo-6-methyl (**3f**). **3k** exhibited most potent HDAC8 inhibition with IC₅₀ value of 2.7 μM with 6- to 16-fold selectivity for HDAC8 over HDAC1, HDAC4 and HDAC6 and even higher selectivity over HDAC3 and HDAC5. This data is not enough to discuss the structure activity relationships, but some primary conclusions can be made. The presence of halogen Br (**3i**, **3h**) and nitro group (**3k**) at para position may lead to enhanced HDAC8 inhibition. Amongst halogens only F containing compounds (**3b**, **3g**) were found to be ineffective against all four subtypes of HDACs, but if it is present along with Br on the same ring (**3f**), it leads to HDAC8 inhibition. Electron withdrawing groups such as NO₂ was found to have HDAC inhibitory potential as compared to electron donating groups (**3c**, **3d**). Amongst brominated derivatives, **3h** and **3i** potency was found to be slightly enhanced if methyl group is present along with Bromine.

Table 1

SAR table of naphthylidene-2,4-TZD derivatives for selectivity between HDAC1, HDAC4, HDAC6 and HDAC8.

IC₅₀ / μM



#	R ₁	R ₂	R ₃	R ₄	R ₅	HDA C1	HDA C2	HDA C3	HDA C4	HDA C5	HDA C6	HDA C8
3a	H	H	H	H	H	> 50	> 50	> 50	> 50	> 50	> 50	44
3b	H	H	F	H	H	> 50	> 50	> 50	> 50	> 50	> 50	> 50
3c	H	H	CH ₃	H	H	> 50	> 50	> 50	> 50	> 50	> 50	> 50
3d	H	H	OCH ₃	H	H	> 50	> 50	> 50	> 50	> 50	> 50	> 50
3e	H	Cl	Cl	H	H	> 50	> 50	> 50	> 50	> 50	> 50	> 50
3f	Br	H	F	H	F	> 50	> 50	> 50	> 50	> 50	> 50	12
3g	F	H	F	H	H	> 50	> 50	> 50	> 50	> 50	> 50	> 50
3h	CH ₃	H	Br	H	H	> 50	> 50	> 50	> 50	> 50	> 50	6.3
3i	H	H	Br	H	H	> 50	> 50	> 50	> 50	> 50	> 50	8.8
3j	H	H	H	CF ₃	H	> 50	> 50	> 50	> 50	> 50	> 50	12
3k	H	H	NO ₂	H	H	23	35	> 50	15	> 50	44	2.7
PCI-34051						3.0*	45*	38*	10*	>50*	18*	0.024*

*Kleinschek, A., et al. (2016). "Potent and Selective Non-hydroxamate Histone Deacetylase 8 Inhibitors." *ChemMedChem* **11**(23): 2598-2606.

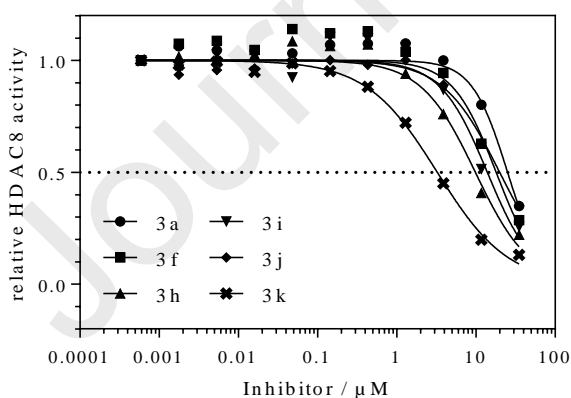


Fig. 3. Dose response curves of indicated compounds against HDAC8. The relative enzyme activity is plotted versus increasing compound concentrations

2.3.2. Thermal Shift Assay

Several promising lead compounds have failed in advanced clinical trials [41-43] and subsequently it has been shown that they do not act in predicted or *in vitro* observed way [44]. Hence target engagement (TE) i.e. extend to which the drug binds to its target protein of enzyme *in situ*, should be studied from the drug development and primary preclinical stage. Thermal shift assay (TSA) is the means by which TE can be established *in vitro* using isolated enzyme to ascertain enzyme-ligand stability with increasing temperature or in cells and tissues to confirm binding. TSA provide characteristic sigmoidal melting curves for a protein. It has been observed that, when ligand binds to protein, melting temperature (T_m) of protein shift to a higher temperature producing thermal shift (ΔT_m), and lead to stabilization of the protein (Fig. 4).

To assess the target engagement of synthesised derivatives, we undertook TSA for derivatives 3a, 3h, 3i and 3k by incubating with recombinant HDAC8 for 1 hour and then exposed to different temperatures ranging from 46 °C to 62 °C. We observed the characteristic sigmoidal curve. Thus, binding of compounds to HDAC8 leads to strong stabilization of the protein-ligand complex with thermal shifts (ΔT_m) of 7 °C and more. We did *in vitro* thermal shift experiments and did not analyze the cell lysates of living cells that were treated with the compounds. However, at stage we can say that the enzyme-ligand complexes are highly stable and, are more likely to bind a desired target, HDAC8 when in whole cells or tissue, making them suitable agents for preclinical developments.

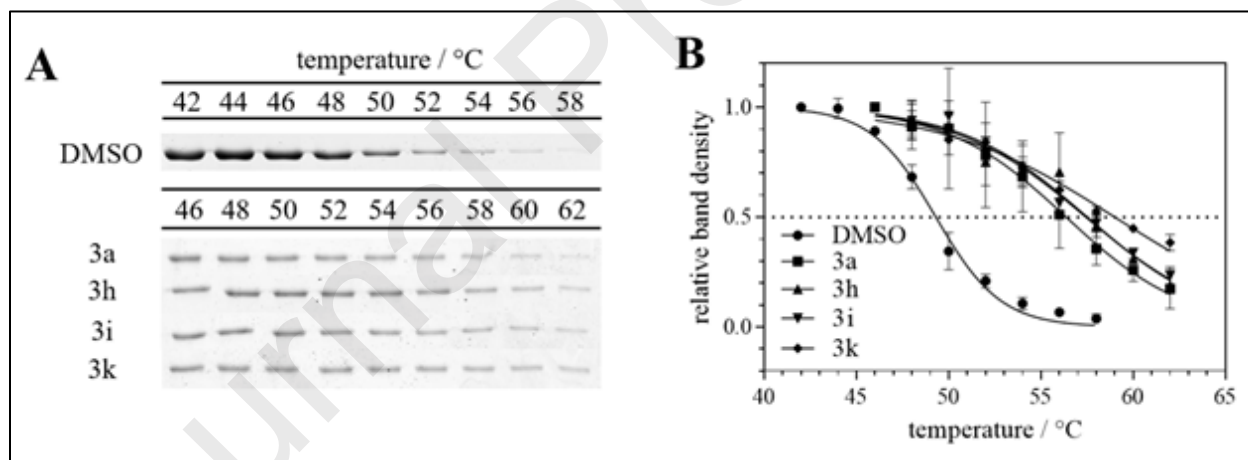


Fig. 4. Thermal stabilization of 2.5 μ M HDAC8 upon binding of 100 μ M of 3a (square), 3h (up-triangle), 3i (down-triangle) and 3k (diamond). Dots denote the control of HDAC8 in the absence of compounds but with matching DMSO concentration. The data points represent means and standard deviations of 3 independent experiments. Compound binding to HDAC8 leads to strong stabilization of the protein-ligand complex with thermal shifts of 7 °C and more.

2.4 *In vitro* anticancer Screening

2.4.1 MTT assay and cell viability

The effects of newly synthesized TZD derivatives 3a-3k, on the viability of normal Human WBCs and cancerous K562 and CEM cells, were assessed by the MTT assay, which has been described as one of the most reliable indicators of metabolic activity of cells and widely used to ascertain

cell viability [45-46]. It relies on the ability of dehydrogenase enzymes to reduce MTT dye to its water insoluble purple coloured formazan salt in the mitochondria of cells. formazan crystals can be finally solubilized and quantified using a spectrophotometer. Since reduction of MTT can only occur in metabolically active cells the level of activity is a measure of the viability of the cells. In this study, Paclitaxel was used as references.

Table 2

IC₅₀ values for compounds 3a-3k on K562 and CEM cell line viability

Compound	IC ₅₀ ^a in μ M	
	K562	CEM
3a	0.42	13.94
3b	0.46	29.40
3c	0.73	38.60
3d	0.52	32.79
3e	0.81	nd ^b
3f	0.97	29.29
3g	0.96	nd ^b
3h	2.05	15.71
3i	1.94	21.22
3j	1.62	nd ^b
3k	nd ^b	nd ^b
Std. Paclitaxel	0.29	15.5

^aData shown is the means of 3 independent experiments.

^bNot determined

We determined the IC₅₀ values corresponding to the concentrations of drug attaining 50% inhibition of cell viability. Paclitaxel was used as standard reference compound whereas untreated cells were used as negative control and the results are presented in **Table 2**. Compounds 3a, 3b, 3c, 3d and 3e were found to exhibit anti-proliferative effects at sub-micromolar concentrations on K562 cell line. CEM cell lines are less sensitive, though the observed activity of the compounds is lesser as compared to K562. IC₅₀ values for CEM cells are around 30 μ M and compound 3a and 3h have exhibited IC₅₀ values less or equal to that of standard drug Paclitaxel. This difference in activity on K562, which is chronic myeloid leukemia cell line and CEM, which is lymphoblastic leukemia cell line, may be due to subtypes of leukemia.

After considering the results of HDAC inhibition and MTT assay, Compounds 3a and 3h was chosen for further evaluation as both exhibited excellent HDAC8 inhibiting activity, 3a exerted high cytotoxicity in both leukemic cell lines with being most cytotoxic compound against K562 cells and compound 3h most cytotoxic compound against CEM cells.

2.4.2 Apoptosis by Flowcytometry

HDAC8 inhibitors have induced necrosis and apoptosis via various mechanisms in different types of solid and hematological cancer cells. PCI-34051, a HDAC8 inhibitor have been found to induce apoptosis in T-cell lymphoma cells by caspase activation [5]. HDAC8 inhibition in gastric carcinoma cells, have reported to induce apoptosis mediated by Bcl-2-modifying factor (BMF) and STAT3 [47]. A selective HDAC8 inhibitor induces Dose-dependent selective apoptosis of CD34+ leukemic stem cells and progenitor cells [7]. The up-regulation of histone deacetylase 8 promotes proliferation and inhibits apoptosis in hepatocellular carcinoma [48].

To examine whether the cytotoxicity induced by **3a** and **3h** was associated with apoptosis, we used annexin V-FITC/ propidium iodide (PI) double staining of K562 and CEM cells treated with indicated compounds and determined rate of apoptosis by flow cytometry. K562 cells are very sensitive to the chosen compounds and treatment of the cells with **3a** and **3h** at IC₅₀ concentration was leading to rapid cell death. In that circumstances getting accurate results were difficult, thus we choose CEM cell line for apoptosis experiments in order to obtain reproducible results. CEM cells exposed to **3a** and **3h** at their IC₅₀ concentrations caused increase of apoptotic cells apoptotic (fig. 5). For **3a** the percentage of apoptotic cells in late and early apoptosis was 41.88 % and 2.80% respectively. In case of **3h** similar results were observed: 42.78% of cells were in the late apoptosis and 1.63%. in early phase of apoptosis. was 1.63%. This result indicates that compound **3a** and **3h** both have the ability to induce apoptotic death in CEM cell line. As apoptosis is a type of cellular death that seems to be safer to patients because of non-inflammatory character and HDAC inhibitors considered for anticancer use all induce apoptosis we conclude studied compounds can proceed to further testing as potential anti-leukemic drug candidate [49] However, further molecular level studies are indicted to unearth the exact mechanism of induction of apoptosis by these compounds.

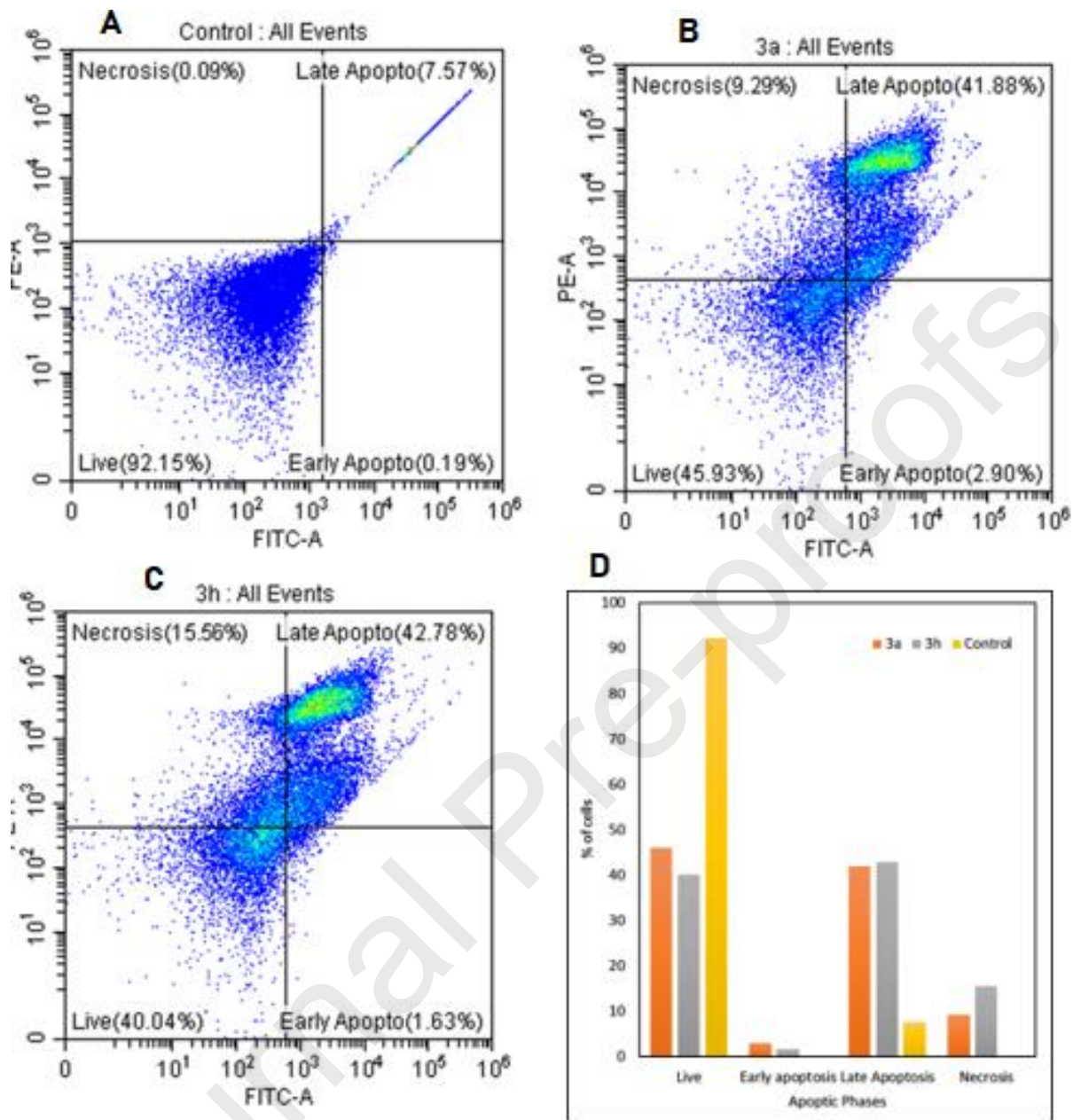


Fig. 5 . Annexin V-FITC/ PI flow cytometry analysis. CEM cells were treated with 3a and 3h at IC₅₀ concentration. After 24 hour cells were stained with annexin V-FITC/PI to distinguish live cells from apoptotic and necrotic cells. Cells considered alive are both Propidium Iodide (PI) & AnnexinV negative, cells in early apoptotic stage are Annexin V positive and PI negative and cells in late apoptotic phase are both PI & Annexin V positive. Dead/necrotic cells are PI positive & Annexin V negative. (A) Cytograms of untreated control CEM cells. (B) Cytograms of 3a treated CEM cells. (C) Cytograms of 3h treated CEM cells. (D) Graphical representation of apoptotic events of untreated, 3a and 3h treated CEM cells.

2.4.3 Cell cycle analysis

Most of pan HDAC inhibitors produce G0/G1 cell cycle arrest and apoptosis through the increased accumulation of acetylated histones, resulting in decreased availability of nuclear DNA to bind to transcription factors and thus decreased transcription that leads to decreases intracellular protein levels the trigger for cell cycle arrest. However, G2/M have been also shown as an outcome of HDAC inhibition. PAC-320, a polyoxometalates compound, is a broad-spectrum HDAC inhibitor have shown potent prostate cancer inhibitory activity mediated by G2/M cell cycle arrest and apoptosis [50]. Not much literature is available about exact behavior of HDAC8 inhibitors in various phases of cell growth and arrest, knockdown of HDAC8 in gastric cancer cells, have been reported to promote G0/G1 arrest and apoptosis[47], whereas knockdown of HDAC8 in lung cancer cell line, A549, Found to promote growth arrest in mitotic G2-M phase[51]. Thus, cell growth arrest has been observed in HDAC8 knockdown cells as well as HDAC8 inhibitor treated cells, but in different phases of growth.

We investigated the effects of **3a** and **3h** on cell cycle using flow cytometric analysis, to find out if it's antiproliferative effects can be attributed to arrest of cells in particular phase (Fig. 6). Treatment of CEM cells with **3a** and **3h** at their IC₅₀ concentrations, resulted in marked increase in the number of cells in G2/M phase and a concomitant decrease in the number of cells in G0/G1 phase as compared to control. For **3a**, the percentage of cells in G2-M phase was found to increase from 3.58% to 35.4%, while the percentage of cells in G0-G1 phase was found to decrease from 73.4% to 37.3% and the percentage of cells in S phase found to be change very slightly as compared to control. For **3h** the percentage of cells in G2-M phase was found to increase from 3.58% to 27.0%, while the percentage of cells in G0-G1 phase was found to decrease from 73.4% to 50.0% and the percentage of cells in S phase found to be remain almost similar as compared to control. Thus, our results may suggest that the reductions in cell growth may be due to direct or indirect interference of **3a** and **3h** with DNA replication resulting block at G2/M cell cycle check point.

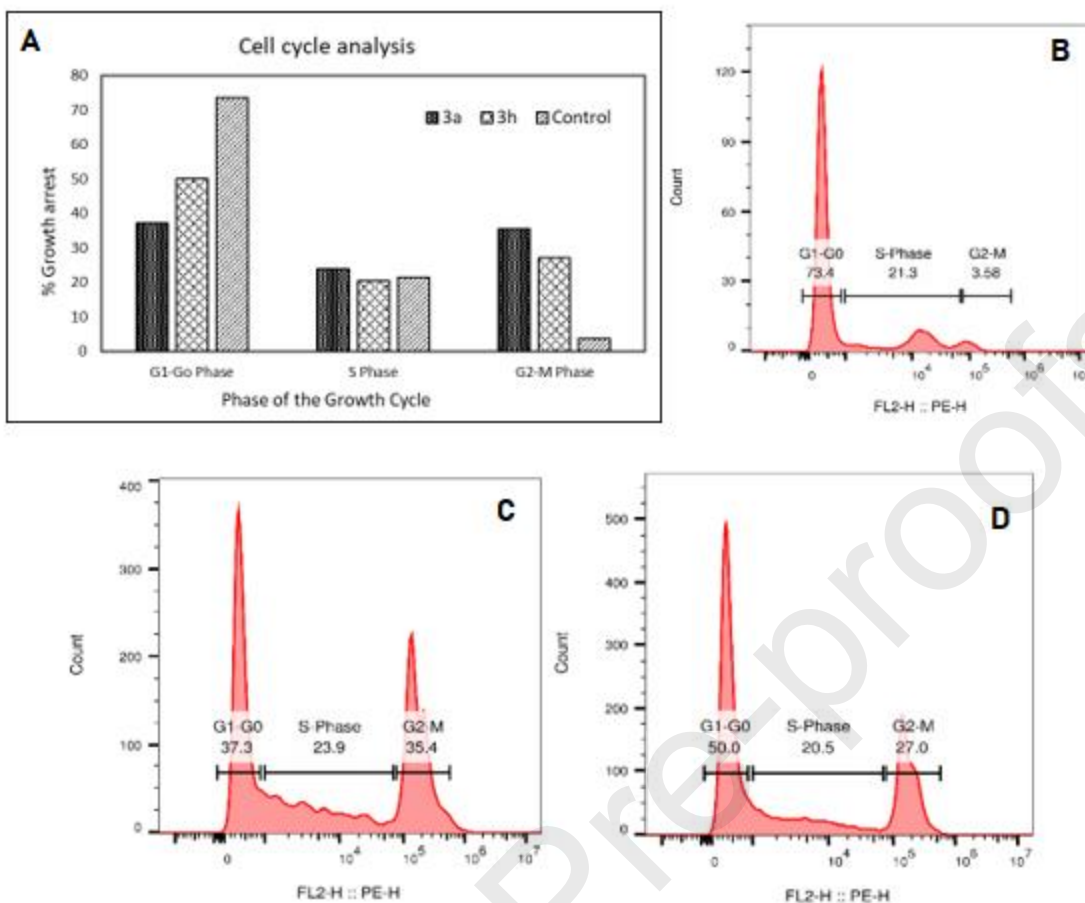


Fig. 6. Effect of 3a and 3h on cell cycle. Cells were treated with compounds for 24 hour, stained with PI, and analysed by flow cytometry. (A) Graphical representation of CEM cells population of in G0/G1, S and G2/M phases of the cell cycle shown as % of all cells. (B) Representative histogram of untreated control cells (C) Representative histogram of 3a treated cells. (D) Representative histogram of 3h showing treated cells.

2.4.4 Assessment of cell viability on non-transformed cells

In leukemia treatment we are looking for medicines that will be lethal to cancer cells and at the same time relatively safe for patient and his normal cells. Since **3a** was most cytotoxic in both K562 and CEM cells, we compared cytotoxicity of the compound against leukemic cells and normal WBCs. The cells were exposed to 2.5, 10, 25, 75 and 100 μM concentrations of **3a** and **3h** for 48 h. to normal WBCs and IC_{50} values, were established. For 3a the IC_{50} value was found to be 67.24 μM , which is 5 times that of IC_{50} for CEM cells ($\text{IC}_{50} = 13.39 \mu\text{M}$) and for 3h it was 152.2 μM , which is 15 times that of IC_{50} for CEM lines, (Fig. 7), which indicates that 3a and 3h could be safer to normal cells.

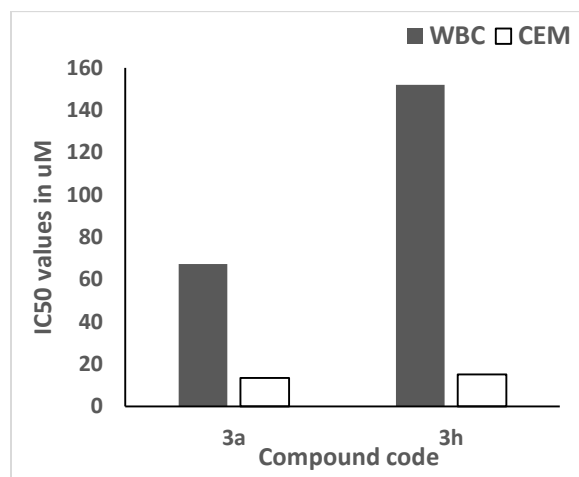


Fig. 7. 3a and 3h inhibits cell proliferation in the human Leukemic cell line, CEM, significantly more than it does in normal WBCs after 48 hours treatment.

2.5 In-silico studies

2.5.1 Docking of 3k into HDAC8 (PDB-ID: 3SFF)

HDAC8 is known as an enzyme with extraordinary malleable binding site suitable to accommodate inhibitors with widely different structures [52-53]. To study the putative molecular determinants of TZD binding to HDAC8, we performed docking studies using three solved crystal structures of HDAC8 (PDB-ID's 1T69, 1VKG and 3SFF), which represent different major conformers of this enzyme [54]. PDB-ID 1T69 shows a complex between HDAC8 and SAHA with one narrow binding channel, 1VKG shows the wide-open conformation of HDAC8 and 3SFF shows a HDAC8 conformation with an open cavity connecting the conventional catalytic site with the entry of the acetate release channel. The far best docking score was obtained with PDB-ID 3SFF (**Table 3**). Surprisingly, not the thiazolidinedione group, but the oxygen of the carboxamide group chelates the zinc cation at the bottom of the catalytic binding pocket. In addition, an oxygen of the nitro group forms a hydrogen bond to a nitrogen of R37 (Fig. 8). The naphthalene moiety of the TZDs appears to be rather movable and to enable pi-pi-interactions with neighbouring F208 and F152 residues lining the binding pocket.

Table 3

Docking scores for 3k within different crystal structures and conformations of HDAC8 using MOE software and AMBER 14 forcefield

PDB-ID	Score
3SFF	-9.5
1T69	-7.3
1VKG	-7.4

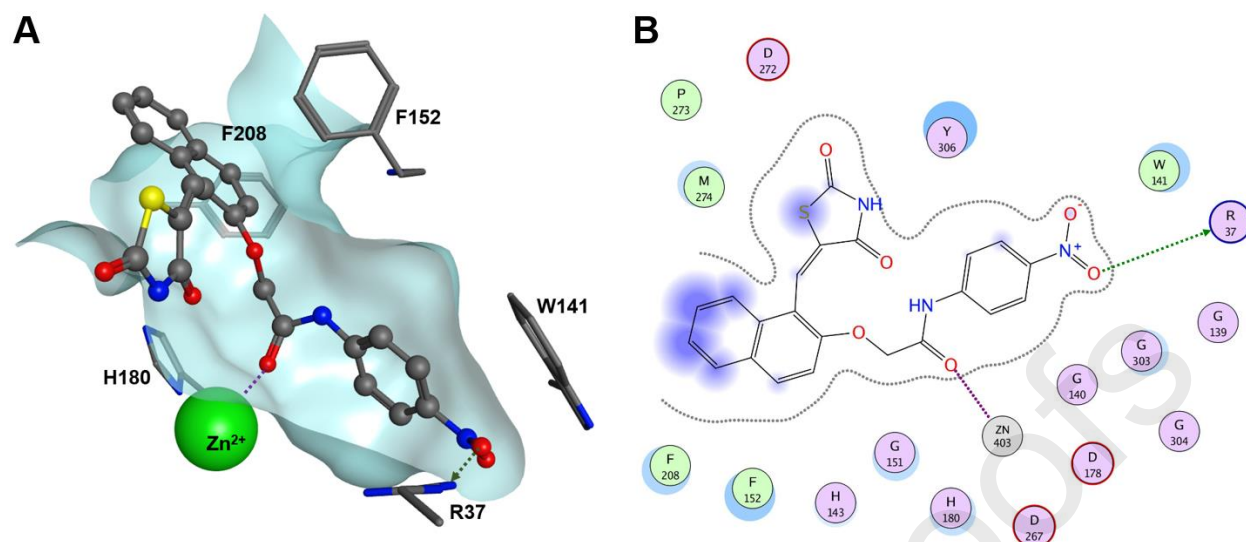


Fig. 8. Best docking pose of **3k** within the binding pocket of HDAC8 (PDB-ID: 3SFF). A) 3D view of binding pocket. B) 2D ligand interactions. Magenta dotted lines indicate metal ion contacts and green arrows hydrogen bonds. The violet or light blue shades denote ligand or receptor exposure, respectively.

The general binding pose of **3k** was confirmed by very similar docking results with analogs, where the para-nitro group was omitted (**3a**) or exchanged against methyl (**3c**), methoxy (**3d**) or bromine (**3i**). The TZDs without nitro-group are no longer able to form a hydrogen bond with R37 resulting in rather weak docking scores (**Table 4**). In contrast, the most potent compound **3k** shows the best docking score based on the hypothesized hydrogen bond between the nitro group and R37. Thus, the docking scores are consistent with the experimental activity of the compounds in terms of IC_{50} -values providing further evidence for the correctness of the putative binding pose of the TZDs within HDAC8.

Table 4

Docking scores and IC_{50} -values for different 3k analogs using MOE software and AMBER 14 forcefield

CPD.	P-SUBSTITUENT	IC_{50} (HDAC8) / μ M	SCORE	CPD.	P-SUBSTITUENT	IC_{50} (HDAC8) / μ M	SCORE
3K	-NO ₂	2.7	-9.5	3A	-H	44	-8.5
3H	-BR + CH ₃ IN ORTHO	6.3	-8.6	3C	-CH ₃	>50	-8.8
3I	-BR	8.8	-8.6	3D	-OCH ₃	>50	-7.9

2.5.2 SwissADME predictions

Calculation of ADME profile is essential part of drug development, but determination of ADME parameters by laboratory experimentations for large number of compounds would be difficult and very time-consuming task. In these circumstances, simulated computer-models provides realistic replacements to experiments [55]. The SwissADME web tool is freely available which gives

access to the fast and robust models for appropriate prediction of physicochemical properties, pharmacokinetic behaviour and drug-likeness. We used SwissADME tool to predict properties of our synthetic derivatives. All the compounds were observed to follow the Lipinski's rule of five (**Table 5**) with 2 violations of molecular weight. All molecules demonstrated $^c\log P$ in the acceptable range of 2.00 to 5.00. Topological polar surface area (TPSA), the surface sum over all polar atoms, primarily oxygen and nitrogen, also including their attached hydrogen atoms, has been shown to be a very good descriptor characterizing drug absorption, including intestinal absorption, bioavailability. Literature implies that $TPSA < 140$ is essential for good absorption. The naphthylidene derivatives exemplified TPSA in the range 109-135 0A . The solubility class predicted indicates that compounds are moderately or poorly soluble, which could be problematic in formulation stage and can be overcome by solubility enhancement techniques such as salt formation. Judging the data, the molecules seem to be drug like and may have good passive oral absorption.

Table 5

SwissADME prediction data.

Code	TPSA ^a	Log P ^b	Log S ^c	ESOL ^d Class	GI ^e absorption	Lipinski #violations	Bioavailability Score
3a	109.8	2.21	-5.08	Moderately soluble	High	0	0.55
3b	109.8	2.59	-5.24	Moderately soluble	High	0	0.55
3c	109.8	2.42	-5.38	Moderately soluble	High	0	0.55
3d	119.03	1.89	-5.16	Moderately soluble	High	0	0.55
3e	109.8	3.17	-6.28	Poorly soluble	High	0	0.55
3f	109.8	3.54	-6.32	Poorly soluble	Low	1	0.55
3g	109.8	2.96	-5.4	Moderately soluble	High	0	0.55
3h	109.8	3.01	-6.3	Poorly soluble	High	0	0.55
3i	109.8	2.8	-5.99	Moderately soluble	High	0	0.55
3j	109.8	3.48	-6.54	Poorly soluble	Low	1	0.55
3k	135.62	2.14	-5.15	Moderately soluble	Low	0	0.55

a- Topological polar surface area b- Log of partition coefficient (P), c- Log solubility, d-estimated aqueous solubility in mg/mL, e- Gastrointestinal

3. Materials and methods

3.1 Chemistry

Commercial reagents were from either S D Fine, Research Lab or Sigma Aldrich and were procured from suppliers in India. Thin layer chromatography was performed on Merck pre-coated Silica Gel 60 F254. Melting points were determined by open capillary method on a VEEGO melting point apparatus and are uncorrected. Infrared spectra were recorded on Shimadzu FT/IR-8400S by direct sampling technique. ^1H and ^{13}C NMR spectra were recorded at 400 MHz on a Bruker instrument using TMS as internal standard and chemical shifts (δ) are reported in ppm. Mass spectra were recorded using LC-MS Agilent Technologies 1260 Infinity instrument.

3.1.1 Procedure for synthesis of 5-((2-hydroxynaphthalen-1-yl) methylene) thiazolidine-2,4-dione (1a)

Compound **1a** was synthesized as per the procedure that we have reported earlier [38]. In short 0.01 moles of 2-hydroxy naphthaldehyde **1** and 0.01 moles of 2,4-thiazolidinedione **2** with catalytic quantity of piperidinium benzoate was refluxed in toluene for 4-5 hours. The reaction mixture was cooled to room temperature and solid separated was collected by filtration, washed with cold toluene, dried and recrystallised from hydroalcoholic mixture.

Yellow crystals; yield 79.5%; m.p, 253 $^{\circ}\text{C}$; ^1H NMR (400 MHz, DMSO d_6) - δ 12.59 (s,1H), δ 10.21 (s,1H), δ 8.04 (s 1H), δ 7.89 (m, 2H), δ 7.79 (d, $J = 8.82$ Hz, 1H), δ 7.57-7.55 (m, 1H), 7.17-7.19 (m, 2H); IR (neat) 3115.14, 1674.27, 1508, 1340 and 1211 cm^{-1} ; anal. calc. for $\text{C}_{14}\text{H}_9\text{NO}_3\text{S}$ C, 61.98; H, 3.34; N, 5.16; O, 17.69; S, 11.82.

3.1.2 General procedure for synthesis of 2a – 2k.

We have previously reported preparation, purification and characterization of 2a-2k in our research papers [38-39]. Briefly, Chloroacetyl chloride (0.1 mol) was added drop wise to a mixture of appropriate amines (0.05 mol) and anhydrous potassium carbonate (K_2CO_3) (0.075 mol) in dichloromethane or chloroform in an ice-cold condition. The reaction mixture was then stirred at room temperature. After completion of reaction, solvent was evaporated under reduced pressure, ice cold water was added to the obtained dry mass and the insoluble product was filtered and dried and purified by recrystallization with appropriate solvents.

3.1.3 General procedure for synthesis of 3a-3k by Condensation of 1a with 2a-2k.

The final compounds 3a-3k were synthesized by stirring compound 0.1 mol of (1a) with 0.1 moles of (2a-2k) for 24 hours, in presence of K_2CO_3 in dimethyl formamide (DMF). The reaction was monitored by TLC. On completion of the reaction, the reaction mixture was poured on crushed ice. The precipitated crude product was filtered, washed with water and purified by column chromatography using ethyl acetate and hexane in appropriate ratio.

3.1.3.1 2-((1-((2,4-dioxothiazolidin-5-ylidene) methyl) naphthalen-2-yl) oxy)-N-phenylacetamide (3a)

Yellow powder; yield 35.8%; m.p, 234 °C(charred); ¹H NMR (400 MHz, DMSO d6): δ 10.51 (s,1H), δ 8.68 (s,1H), δ 8.48-8.46 (d, J = 8.0 Hz, 1H), δ 8.04-8.06 (d, J = 8.0 Hz, 1H), 7.98-8.00 (d, J = 8.0 Hz, 1H), δ 7.71-7.73 (m, 1H), δ 7.65-7.67 (m, 2H), δ 7.57-7.61 (m, 1H), δ 7.49-7.51 (d, J = 8.0 Hz, 1H), δ 7.32-7.36 (t, J = 8.0 Hz, 2H), δ 7.06-7.10 (t, J = 8.0 Hz, 1H), δ 4,15 (s, 2H); ¹³C NMR (400MHz, DMSO d6): δ 158.24, 150.38, 113.23, 138.67, 116.28, 129.95, 131.33, 123.66, 127.67, 122.08, 131.59, 166.38, 40.06, 128.83, 122.08, 128.66, 127.93, 126.03, 119.18; IR (neat) 3340.82, 1693.56, 1672.34, 1494.88, 1325.14 and 1213.72 cm⁻¹; Theoretical mass: 404.08, LC-MS (m/z, I %): 403.1 [(M-H)⁺, 100]; anal. calc. for C₁₄H₉NO₃S: C, 65.33; H, 3.99; N, 6.93; O, 15.82; S, 7.93.

3.1.3.2 2-((1-((2,4-dioxothiazolidin-5-ylidene) methyl) naphthalen-2-yl) oxy)-N-(4-fluorophenyl) acetamide (3b)

Yellow powder; yield 30.3%; m.p, 259 °C (charred); ¹H NMR (400 MHz, DMSO d6): δ 10.48 (s,1H), δ 8.77 (s,1H), δ 8.53-8.55 (d, J = 8.0 Hz, 1H), δ 8.13-8.15 (d, J = 8.0 Hz, 1H), 8.06-8.07 (d, J = 4.0 Hz, 1H), δ 7.74-7.77 (t, J = 6.0 Hz, 1H), δ 7.65-7.60 (m, 4H), δ 7.13-7.16 (t, J = 6.0 Hz, 2H), δ 4,12 (s, 2H); ¹³C NMR (400MHz, DMSO d6): δ 159.49, 158.27, 111.45, 131.68, 125.74, 126.10, 127.74, 127.99, 128.73, 129.66, 109.04, 150.46, 166.40, 54.93, 122.17, 113.30, 131.46, 130.02; IR (neat) 1689, 1284, 1213, 3335, 1618 and 1099 cm⁻¹; Theoretical mass: 422.07, LC-MS (m/z, I %): 421.1 [(M-H)⁺, 100]; anal. calc. for C₂₂H₁₅FN₂O₄S: C, 62.55; H, 3.58; F, 4.50; N, 6.63; O, 15.15; S, 7.59.

3.1.3.3 2-((1-((2,4-dioxothiazolidin-5-ylidene)methyl)naphthalen-2-yl) oxy)-N-(p-tolyl) acetamide (3c)

Yellow powder; yield 25.97%; m.p, 220.2 °C (charred); ¹H NMR (400 MHz, DMSO d6): δ 10.38 (s,1H), δ 8.74 (s,1H), δ 8.53-8.51 (d, J = 8.0 Hz, 1H), δ 8.10-8.12 (d, J = 8.0 Hz, 1H), 8.03-8.05 (d, J = 4.0 Hz, 1H), δ 7.72-7.76 (m, 1H), δ 7.57-7.64 (m, 2H), δ 7.48-7.50 (m, 3H), δ 7.10-7.12 (m, 1H), δ 4.11 (s, 2H), 2.23 (s, 3H); ¹³C NMR (400MHz, DMSO d6): δ 158.29, 150.49, 113.34, 131.44, 127.79, 128.05, 126.15, 128.78, 129.18, 130.06, 119.17, 136.15, 166.07, 40.07, 131.70, 122.21, 129.18, 132.61; IR (neat) 1695, 1246, 1213, 3342, 1555 and 1170 cm⁻¹; Theoretical mass: 418.1, LC-MS (m/z, I %): 416.8[(M-H)⁺, 100]; anal. calc. for C₂₃H₁₈N₂O₄S: C, 66.01; H, 4.34; N, 6.69; O, 15.29; S, 7.66.

3.1.3.4 2-((1-((2,4-dioxothiazolidin-5-ylidene)methyl)naphthalen-2-yl) oxy)-N-(4-methoxyphenyl) acetamide (3d)

Buff Yellow powder; yield 30%; m.p, 231.9 °C; ¹H NMR (400 MHz, DMSO d6): δ 10.36 (s,1H), δ 8.69 (s,1H), δ 8.47-8.49 (d, J = 8.0 Hz, 1H), δ 8.05-8.07 (d, J = 8.0 Hz, 1H), 8.01-7.99 (d, J = 8.0 Hz, 1H), δ 7.70-7.74 (m, 1H), δ 7.51-7.62 (m, 4H), δ 6.89-6.91(m, 2H), δ 4.11 (s, 2H), δ 3.71 (s, 3H); ¹³C NMR (400MHz, DMSO d6): δ 157.40, 154.59, 113.06, 130.94, 119.90, 127.85, 127.11, 125.21, 126.86, 125.02, 129.14, 164.98, 54.25, 130.42, 121.26, 115.47, 149.54; IR (neat) 1691, 1240, 1213, 3336, 1545 and 1168 cm⁻¹; Theoretical mass: 434.09, LC-MS (m/z, I %): 433 [(M-H)⁺, 100]; anal. calc. for C₂₃H₁₈N₂O₅S: C, 63.58; H, 4.18; N, 6.45; O, 18.41; S, 7.38.

3.1.3.5 N-(3,4-dichlorophenyl)-2-((1-((2,4-dioxothiazolidin-5-ylidene) methyl) naphthalen-2-yl)oxy) acetamide (**3e**)

Yellow powder; yield 30%; m.p, 293.6 °C(charred); ¹H NMR (400 MHz, DMSO d6): δ 10.73 (s,1H), δ 8.75 (s,1H), δ 8.52-8.54 (d, J = 8.0 Hz, 1H), δ 8.13-8.15 (d, J = 8.0 Hz, 1H), 8.05-8.07 (d, J = 8.0 Hz, 1H), δ 7.96-7.97 (m, 1H), δ 7.73-7.77 (m, 1H), δ 7.63-7.65(m, 1H), δ 7.56-7.61(m, 2H), δ 7.48-7.51(m, 1H), δ 4.14 (s, 2H); ¹³C NMR (400MHz, DMSO d6): δ 158.31, 150.69, 113.32, 138.70, 119.24, 130.07, 128.81, 127.83, 125.10, 126.18, 122.23, 130.79, 166.95, 40.07, 131.90, 131.04, 128.09, 120.35, 125.31; IR (neat) 1587, 1319, 1213, 3338, 1531 and 736 cm⁻¹; Theoretical mass: 472.01, LC-MS (m/z, I %): 471[(M-H)⁺, 100]; anal. calc. for C₂₂H₁₄Cl₂N₂O₄S: C, 55.82; H, 2.98; Cl, 14.98; N, 5.92; O, 13.52; S, 6.77.

3.1.3.6 N-(2-bromo-4,6-difluorophenyl)-2-((1-((2,4-dioxothiazolidin-5-ylidene)methyl) naphthalen-2-yl)oxy) acetamide (**3f**)

Yellow powder; yield 31.2%; m.p, 268.5 °C(charred); ¹H NMR (400 MHz, DMSO d6): δ 10.15 (s,1H), δ 8.73 (s,1H), δ 8.53 (s,1H), δ 8.05-8.12 (m, 2H), δ 7.43-7.74 (m, 5H), δ 4.19 (s, 2H); ¹³C NMR (400MHz, DMSO d6): δ 158.40, 150.67, 113.22, 138.20, 119.20, 130.17, 127.81, 124.20, 126.18, 122.23, 130.79, 166.95, 41.07, 132.90, 131.14, 128.19, 120.32, 125.33; IR (neat) 1587, 1319, 1213, 3338, 1531 and 736 cm⁻¹; Theoretical mass: 517.97, LC-MS (m/z, I %): 518.9 [(M+H)⁺, 100]; anal. calc. for C₂₂H₁₃BrF₂N₂O₄SC, 50.88; H, 2.52; Br, 15.39; F, 7.32; N, 5.39; O, 12.32; S, 6.17.(¹³C NMR and IR is not available, data entered is approximate)

3.1.3.7 N-(2,4-difluorophenyl)-2-((1-((2,4-dioxothiazolidin-5-ylidene) methyl) naphthalen-2-yl)oxy) acetamide (**3g**)

Yellow powder; yield 24.69%; m.p, 231.6 °C(charred); ¹H NMR (400 MHz, DMSO d6): δ 10.26 (s,1H), δ 8.73 (s,1H), δ 8.51-8.53 (m, 1H), δ 8.11-8.13 (d, J = 8.0 Hz, 1H), 8.04-8.06 (d, J = 8.0 Hz, 1H), δ 7.80-7.86 (m, 1H), δ 7.73-7.76 (m, 1H), δ 7.58-7.65(m, 2H), δ 7.56-7.61(m, 2H), δ 7.31-7.36(t, J = 10.0 Hz, 1H), δ 7.03-7.07 (m, 1H), δ 4.21 (s, 2H); ¹³C NMR (400MHz, DMSO d6): δ 158.30, 150.54, 104.23, 130.06, 111.30, 127.80, 126.15, 125.64, 116.41, 125.44, 113.33, 128.03, 166.92, 40.07, 111.11, 131.76, 104.24, 131.62, 111.11, 122.18; IR (neat) 1666, 1317, 1213, 3338, 1593 and 1006 cm⁻¹; Theoretical mass: 440.06, LC-MS (m/z, I %): 439 [(M-H)⁺, 100]; anal. calc. for C₂₂H₁₄F₂N₂O₄S: C, 60.00; H, 3.20; F, 8.63; N, 6.36; O, 14.53; S, 7.28.

3.1.3.8 N-(4-bromo-2-methylphenyl)-2-((1-((2,4-dioxothiazolidin-5-ylidene) methyl) naphthalen-2-yl)oxy) acetamide (**3h**)

Deep yellow powder; yield 35%; m.p, 253 °C(charred); ¹H NMR (400 MHz, DMSO d6): δ 10.49 (s,1H), δ 8.71 (s,1H), δ 8.50-8.52 (d, J = 8.0 Hz, 1H), δ 8.07-8.10 (d, J = 8.0 Hz, 1H), 8.01-8.03 (d, J = 8.0 Hz, 1H), δ 7.71-7.74 (t, J = 6.0 Hz, 1H), δ 7.53-7.63 (m, 2H), δ 7.17-7.25 (m, 2H), δ 6.65-6.67 (d, J = 6.0 Hz, 1H), δ 4.14 (s, 2H), δ 2.52 (s, 2H); ¹³C NMR (400MHz, DMSO d6): δ 158.27, 150.46, 113.30, 139.82, 128.73, 127.74, 126.10, 122.17, 125.74, 116.36, 166.40, 54.93, 131.68; IR (neat) 1672, 1251, 1201, 3390, 1604, 1450 and 1072 cm⁻¹; Theoretical mass: 496.01, LC-MS (m/z, I %): 496.9 [(M+H)⁺, 100]; anal. calc. for C₂₃H₁₇BrN₂O₄S: C, 58.79; H, 3.36; N, 9.35; O, 21.36; SC, 55.54; H, 3.45; Br, 16.07; N, 5.63; O, 12.87; S, 6.45, 7.13

3.1.3.9 N-(4-bromophenyl)-2-((1-((2,4-dioxothiazolidin-5-ylidene) methyl) naphthalen-2-yl) oxy) acetamide (**3i**)

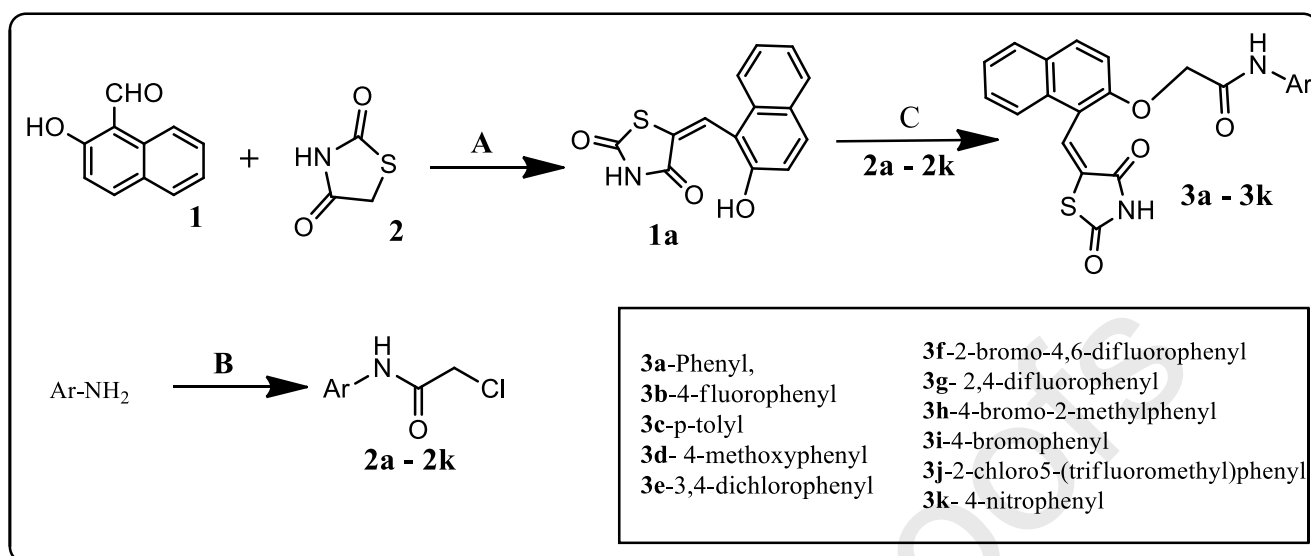
Dark yellow powder; yield 26%; m.p, 262.6 °C(charred); ¹H NMR (400 MHz, DMSO d6): δ 10.59 (s,1H), δ 8.75 (s,1H), δ 8.51-8.53 (d, J = 8.0 Hz, 1H), δ 8.12-8.14 (d, J = 8.0 Hz, 1H), 8.04-8.06 (d, J = 8.0 Hz, 1H), δ 8.03-8.05 (d, J = 8.0 Hz, 1H), δ 7.73-7.77 (t, J = 8.0 Hz, 1H), δ 7.57-7.65 (m, 5H), δ 7.48-7.50 (m, 2H), δ 4.13 (s, 2H); ¹³C NMR (400MHz, DMSO d6): δ 158.30, 150.59, 113.33, 138.01, 115.25, 128.09, 127.81, 126.17,122.21, 125.60,121.09, 128.81, 166.57, 40.07, 131.66, 121.09, 130.07, 116.43; IR (neat) 1672, 1319, 1213, 3346, 1589 and 536 cm⁻¹; Theoretical mass: 481.99, LC-MS (m/z, I %): 482.9 [(M+H)⁺, 100]; anal. calc. for C₂₂H₁₅BrN₂O₄S: C, 54.67; H, 3.13; Br, 16.53; N, 5.80; O, 13.24; S, 6.63.

3.1.3.10 N-(2-chloro-5-(trifluoromethyl) phenyl)-2-((1-((2,4-dioxothiazolidin-5-ylidene) methyl) naphthalen-2-yl) oxy) acetamide (**3j**)

Dark yellow powder; yield 28.57%; m.p, 238.6 °C(charred); ¹H NMR (400 MHz, DMSO d6): δ 10.23 (s,1H), δ 8.76 (s,1H), δ 8.55-8.57 (d, J = 8.0 Hz, 1H), δ 8.17 (m, 1H), 8.12-8.14 (d, J = 8.0 Hz, 1H), δ 8.04-8.06 (m, 1H), δ 7.72-7.76 (m, 2H), δ 7.53-7.65 (m, 3H), δ 4.29 (s, 2H); ¹³C NMR (400MHz, DMSO d6): δ 158.34, 150.71, 113.32, 135.40, 122.27, 130.05, 128.77, 128.19, 127.81, 128.01, 126.15, 130.80, 167.51, 40.07, 131.91, 127.86, 129.99, 125.20, 116.40; IR (neat) 1678, 1359, 1213, 3473, 1587, 1327 and 804 cm⁻¹; Theoretical mass: 506.03, LC-MS (m/z, I %): 505 [(M-H)⁺, 100]; anal. calc. for C₂₃H₁₄ClF₃N₂O₄S: C, 54.50; H, 2.78; Cl, 6.99; F, 11.24; N, 5.53; O, 12.63; S, 6.33.

3.1.3.11 2-((1-((2,4-dioxothiazolidin-5-ylidene) methyl) naphthalen-2-yl) oxy)-N-(4-nitrophenyl) acetamide (**3k**)

Deep yellow powder; yield 25%; m.p, 264 °C(charred); ¹H NMR (400 MHz, DMSO d6): δ 11.05 (s,1H), δ 8.75 (s,1H), δ 8.51-8.53 (d, J = 8.0 Hz, 1H), δ 8.20-8.23 (m, 2H), 8.10-8.12 (d, J = 8.0 Hz, 1H), δ 8.03-8.05 (d, J = 8.0 Hz, 1H), δ 7.84-7.87 (d, J = 12.0 Hz, 2H), δ 7.73-7.77 (t, J = 8.0 Hz, 1H), δ 7.62-7.64(m, 1H), δ 7.56-7.60 (m, 1H), δ 4.21 (s, 2H); ¹³C NMR (400MHz, DMSO d6): δ 158.28, 150.66, 113.27, 142.40, 128.07, 127.79, 126.13, 122.17, 125.18, 118.89, 128.75, 167.43, 40.07, 132.23, 116.38, 125.02, 131.87; IR (neat) 1680, 1257, 1211, 3433, 1597, 1550 and 1006 cm⁻¹; Theoretical mass: 449.07, LC-MS (m/z, I %): 448 [(M-H)⁺, 100]; anal. calc. for C₂₂H₁₅N₃O₆S: C, 58.79; H, 3.36; N, 9.35; O, 21.36; S, 7.13.



Scheme 1. Reagents and conditions. **A:** Toluene, Piperidinium acetate- Reflux 2-3 h. **B:** Chloroacetyl Chloride, DCM, K_2CO_3 , stirring at RT. overnight, **C:** DMF, K_2CO_3 - stirring at RT. overnight.

3.2 *In vitro* HDAC screening

3.2.1 HDAC enzyme inhibition Assay

Recombinant HDACs 1, 2, 3, 5 and 6 were purchased at BPS Bioscience. Recombinant HDAC8 was produced as described recently [56]. HDAC8 was produced in *E. coli* (BL21) DE3 pLysS cells using a pET14b vector containing codon-optimized human HDAC8. Recombinant cHDAC4 was expressed using a pET14b vector (Novagen, EMD Millipore) containing the codon-optimized catalytic domain of human HDAC4.

A serial dilution of inhibitor in assay buffer (25 mM Tris-HCl, pH 8.0, 75 mM KCl, 0.001 % Pluronic F-127) was incubated with HDAC in a black 96-well microtiter half-area plate (Greiner) for 60 min at 30 °C. Afterwards the reaction was initiated by the addition of 20 μ M Boc-Lys(trifluoroacetyl)-AMC (Bachem) as substrate for HDAC4, 5 and 8 and 50 μ M Boc-Lys(acetyl)-AMC as substrate for HDAC1, 2, 3 and 6. After incubation for 60 min at 30 °C, the reaction was stopped by the addition of 1.7 μ M SATFMK for HDAC4, 5 and 8 and 4.2 μ M suberoylanilide hydroxamic acid (SAHA, Cayman Chemical Company) for HDACs 1,2,3 and 6. The deacetylated substrate was converted into a fluorescent product by the addition of 0.4 mg/ml trypsin (Applichem). The release of AMC was followed in a microplate reader (PheraStar Plus, BMG Labtech) at 450 nm (λ_{Ex} = 350 nm) and correlated to enzyme activity. Dose-response curves were generated by using GraphPad Prism and fitted to a four parameters logistic function to obtain IC_{50} values [57]:

$$EA = E_0 + \frac{(E_{max} - E_0)}{1 + 10^{(\log(IC_{50}) - x) * h}}$$

in which EA is the enzyme activity at a given inhibitor concentration x , E_{\max} and E_0 are the enzyme activities determined at zero and complete inhibition, respectively. IC_{50} denotes the inhibitor concentration at which half the enzyme is inhibited and h is the slope of the curve.

3.2.2 Thermal shift assay

The thermal shift assay was performed as described recently [58]. In short, 2.5 μ M recombinant HDAC8 was incubated with 100 μ M of the indicated inhibitor for 1h at 30°C and afterwards aliquoted in PCR-Tubes. Each tube was tempered for 10 min at the indicated temperature and subsequent centrifuged. The soluble protein phase was then conducted to SDS-PAGE and band densities were quantified using Image Studio Lite (LiCor) and plotted against the temperature.

3.3 *In vitro* anticancer Screening

3.3.1 Cell cultures

K562 cell line (chronic myeloid leukaemia) was purchased from National Centre for Cell Sciences (NCCS), Pune. CEM (acute T-cell lymphoblastic leukemia) was obtained from the Department of Biochemistry Indian Institute of Science, Bangalore. K562 and CEM cells were maintained as suspension in RPMI 1640 medium (Thermo fisher scientific) supplemented with 10% fetal bovine serum (Gibco, Invitrogen) and 1% antibiotic–antimycotic 100X solution (100 units/mL of penicillin, 100 μ g/mL of streptomycin, and 0.25 μ g/mL of Gibco Amphotericin B). Cells were maintained in a humidified 5% CO_2 atmosphere at 37°C.

3.3.2 Cytotoxicity assay

MTT assay was used to determine cytotoxic potential of **3a** to **3k** on leukemic cell lines, K562 and CEM. The assay was performed as described earlier [59]. Briefly, the cells were seeded at a density of approximately 5×10^3 cells/well in a 96-well flat-bottom micro-plate and maintained at 37°C in 95% humidity and 5% CO_2 overnight. Different concentrations of compounds were diluted in DMSO and were added to the cells. The final concentration of DMSO in the experiments was less than 1.5% and showed no cell toxicity. The cells were incubated with the compounds for 48 h. Next, 96-well plates were centrifuged at 300 g, 4°C for 5 minutes and cells in well were washed with phosphate buffer solution twice., 20 μ L of the MTT staining solution (5mg/ml in phosphate buffer solution) was added to each well and the plate was incubated at 37°C. After 4 h, 100 μ L of dimethyl sulfoxide (DMSO) was added to each well to dissolve the formazan crystals, and absorbance was recorded with a 570 nm using micro plate reader.

3.3.3 Apoptosis by flow cytometry

The induction of apoptosis produced by compound **3a** and **3h** was studied by flow cytometry as described earlier [60]. Cells were seeded in a 24-well flat bottom micro plate and incubated at 37°C in 5% CO_2 atmosphere for 24 h. The media was replaced with fresh media and then for 24 h, the cells were treated with IC_{50} concentration of **3a** and **3h**. Untreated cells were used as negative control. Post incubation, cells were washed with PBS, Centrifuge for 5 minutes at 300 g at 4°C,

and supernatant was discarded. Cell pellets were re-suspended in ice-cold 1X Binding Buffer, 1 μ L of annexin V-FITC solution and 5 μ L PI (propidium iodide) were added and mixed. Tubes were kept on ice and incubated for 15 minutes in the dark. 400 μ L of ice-cold 1X binding buffer was added and cell preparations were analyzed using flow cytometer (BD Accuri™ C5 flow cytometer, BD Biosciences, CA, USA). FlowJo software was used for data analysis (version 10.1, Ashland, OR, USA).

3.3.4 Flow cytometry analysis of cell cycle

Cells were seeded in a 24-well flat bottom micro plate and incubated overnight at 37°C in CO₂ incubator for 24 h. The media was replaced with fresh media and then for 24 h., the cells were treated with IC₅₀ concentration of **3a** and **3h**. Untreated cells were used as negative control. Post incubation, cells were washed with PBS, Centrifuge for 5 minutes at 300g at 4°C, and supernatant was discarded. Cell were re-suspended in 0.5 ml PBS. The cells were fixed on ice in 4.5 ml of ice cold 70 % ethanol for 2 h, centrifuged for 5min at 200 x g at 4°C and ethanol was decanted. Then the cell pellets were Suspended in 5 ml PBS for 1 minute, centrifuged for 5min at 200 x g at 4°C and treated with 1 ml propidium iodide staining solution for 15 mins at 37°C. Cell were analyzed within 30 min. (BD Accuri™ C5 flow cytometer, BD Biosciences, CA, USA). Obtained data was analyzed using FlowJo software (version 10.1, Ashland, OR, USA).

3.3.5 Assessment of cell viability on non- transformed cells

Normal human WBCs were isolated from the peripheral blood of healthy blood donor. The study was approved by appropriate Institutional Review Board. Blood was drawn during routine diagnostic procedures after written informed consent was obtained from patient. The blood samples were spun in a centrifuge and WBCs were isolated from the “buffy coat” fraction. Cells were maintained in a humidified 5% CO₂ atmosphere at 37°C.

Effect of the treatment of compounds **3a** and **3h** on the viability of normal human WBCs, were determined by using MTT assay as described above in cytotoxicity assay. Wherein normal WBCs were treated with increasing concentrations of **3a** and **3h** from 2.5 to 100 μ M for 48h to determine the difference in the cell viabilities of normal cells and finally to calculate IC₅₀ value.

3.4 In silico studies

3.4.1 Molecular docking and energy minimization

Modeling, preparation and visualization of structural data as well as molecular docking was performed using MOE 2019 software (Chemical Computing Group ULC, Canada). Three crystal structures representing significant conformations of HDAC8 (PDB-ID's 1T69, 1VKG, 3SFF) were obtained from RCSB Protein Data Bank. The structure files were loaded into the program and subjected to structure preparation including 3D protonation for subsequent docking. The partial charges of all protein and ligand atoms were calculated using the implemented Amber14 force field. Molecular docking was performed choosing the triangle matcher for placement of the ligand in the binding site and ranked with the London dG scoring function. The best 30 poses were passed

to the refinement and energy minimization in the pocket using the induced fit method and then rescored with the GBVI/WSA dG scoring function.

3.4.2 SwissADME predictions

SwissADME is freely available but reliable online tool which can be used to predict physicochemical, pharmacokinetic and bioavailability of the synthetic molecules, simply by providing structural inputs. The web address of the tool is <http://www.swissadme.ch/index.php#>.

4. Conclusion:

We have successfully synthesized and characterised a series of 5-naphthylidene-2,4-thiazolidinedione derivatives as selective non-hydroxamate HDAC8 inhibitors. Among the synthesized derivatives, compounds **3a**, **3f** and **3h-3j** were found to be selective for HDAC8 in HDAC screening of HDAC1,2,3, 4, 5, 6 and 8. In TSA, all the screened derivatives showed shift in ΔT_m of 7 °C and more. In cytotoxicity assays in K562 and CEM cell lines, **3a** exhibited most potent cytotoxic effects and was found to be safer in normal WBCs. **3a** and **3h** both lead to cell cycle arrest in G2/M phase and was able to induce apoptosis in CEM cells (Fig. 9). Docking studies correlated well with the HDAC inhibitory concentrations and carboxylate group was found to interact with zinc at zinc binding site. Crystallographic studies need to be performed to determine actual interactions at active site of HDAC8. Given that Compound 3h exhibits HDAC8 selectivity and potent antitumor effects in vitro, further in-depth studies on these molecules are expected to give rise to potent leads.

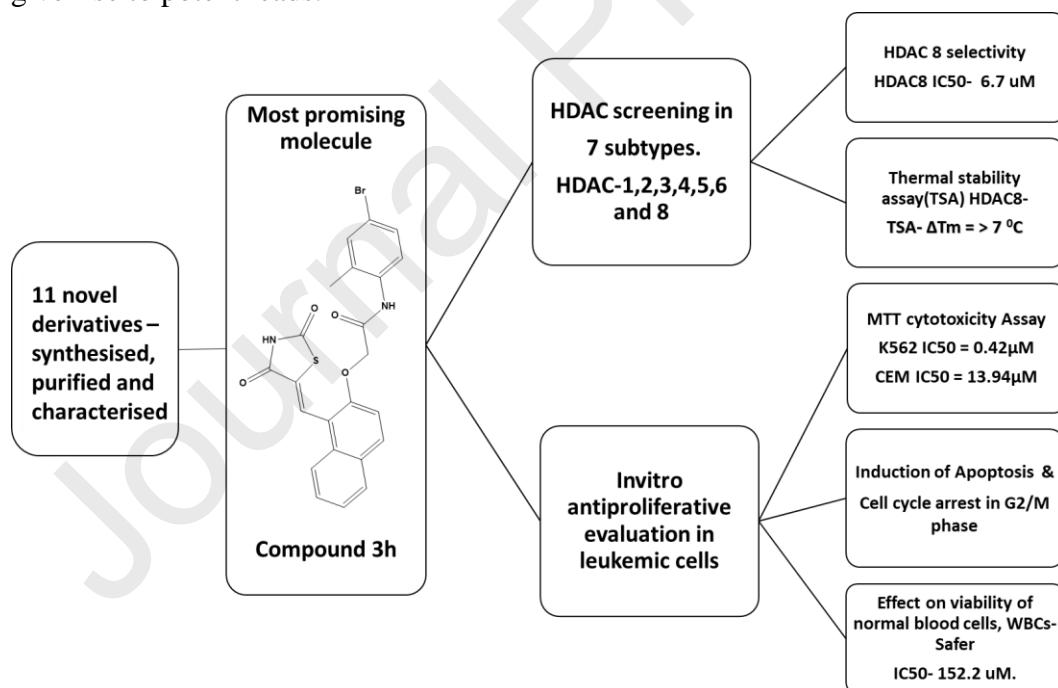


Fig. 9. Schematic representation of results.

Conflict of interest

The authors declare that they have no conflict of interest.

Acknowledgement:

This study was supported by Indo-Poland joint research programme grant from Department of Science and Technology (DST) with reference number DST/INT/Pol/P-27/2016.

Abbreviations

TZD- Thiazolidinedione

HDAC- Histone deacetylase

DMF- Dimethyl Formamide

DCM- Dichloromethane

NMR- Nuclear magnetic resonance spectroscopy

IR- Infrared Spectroscopy

DMEM- Dulbecco's Modified Eagle Medium

MTT- 3-(4,5-dimethylthiazol-2-yl)-2,5-diphenyltetrazolium bromide

FBS- fetal calf serum

RT- room temperature

References:

1. Sharma, S., Kelly, T.K., Jones, P.A., 2010. Epigenetics in cancer. *Carcinogenesis* 31, 27–36. <https://doi.org/10.1093/carcin/bgp220>
2. Mann, B.S., Johnson, J.R., Cohen, M.H., Justice, R., Pazdur, R., 2007. FDA Approval Summary: Vorinostat for Treatment of Advanced Primary Cutaneous T-Cell Lymphoma. *The Oncologist* 12, 1247–1252. <https://doi.org/10.1634/theoncologist.12-10-1247>
3. Laubach, J.P., Moreau, P., San-Miguel, J.F., Richardson, P.G., 2015. Panobinostat for the Treatment of Multiple Myeloma. *Clinical Cancer Research* 21, 4767–4773. <https://doi.org/10.1158/1078-0432.CCR-15-0530>
4. Oehme, I., Deubzer, H.E., Lodrini, M., Milde, T., Witt, O., 2009. Targeting of HDAC8 and investigational inhibitors in neuroblastoma. *Expert Opinion on Investigational Drugs* 18, 1605–1617. <https://doi.org/10.1517/14728220903241658>
5. Balasubramanian, S., Ramos, J., Luo, W., Sirisawad, M., Verner, E., Buggy, J.J., 2008. A novel histone deacetylase 8 (HDAC8)-specific inhibitor PCI-34051 induces apoptosis in T-cell lymphomas. *Leukemia* 22, 1026–1034. <https://doi.org/10.1038/leu.2008.9>
6. Chakrabarti, A., Oehme, I., Witt, O., Oliveira, G., Sippl, W., Romier, C., Pierce, R.J., Jung, M., 2015. HDAC8: a multifaceted target for therapeutic interventions. *Trends in Pharmacological Sciences* 36, 481–492. <https://doi.org/10.1016/j.tips.2015.04.013>
7. Chakrabarti, A., Melesina, J., Kolbinger, F.R., Oehme, I., Senger, J., Witt, O., Sippl, W., Jung, M., 2016. Targeting histone deacetylase 8 as a therapeutic approach to cancer and neurodegenerative diseases. *Future Medicinal Chemistry* 8, 1609–1634. <https://doi.org/10.4155/fmc-2016-0117>
8. Amin, S.A., Adhikari, N., Jha, T., 2017. Structure–activity relationships of hydroxamate-based histone deacetylase-8 inhibitors: reality behind anticancer drug discovery. *Future Medicinal Chemistry* 9, 2211–2237. <https://doi.org/10.4155/fmc-2017-0130>

9. Amin, Sk.A., Adhikari, N., Jha, T., 2018. Structure-activity relationships of HDAC8 inhibitors: Non-hydroxamates as anticancer agents. *Pharmacological Research* 131, 128–142. <https://doi.org/10.1016/j.phrs.2018.03.001>
10. Shen, S., Kozikowski, A.P., 2016. Why Hydroxamates May Not Be the Best Histone Deacetylase Inhibitors-What Some May Have Forgotten or Would Rather Forget? *ChemMedChem* 11, 15–21. <https://doi.org/10.1002/cmdc.201500486>
11. Johnstone, R.W., 2002. Histone-deacetylase inhibitors: novel drugs for the treatment of cancer. *Nat Rev Drug Discov* 1, 287–299. <https://doi.org/10.1038/nrd772>
12. Marks, P.A., Rifkind, R.A., Richon, V.M., Breslow, R., Miller, T., Kelly, W.K., 2001. Histone deacetylases and cancer: causes and therapies. *Nat Rev Cancer* 1, 194–202. <https://doi.org/10.1038/35106079>
13. Mai, A., Massa, S., Rotili, D., Cerbara, I., Valente, S., Pezzi, R., Simeoni, S., Ragno, R., 2005. Histone deacetylation in epigenetics: An attractive target for anticancer therapy. *Med. Res. Rev.* 25, 261–309. <https://doi.org/10.1002/med.20024>
14. Miller, T.A., Witter, D.J., Belvedere, S., 2003. Histone Deacetylase Inhibitors. *J. Med. Chem.* 46, 5097–5116. <https://doi.org/10.1021/jm0303094>
15. Whitehead, L., Dobler, M.R., Radetich, B., Zhu, Y., Atadja, P.W., Claiborne, T., Grob, J.E., McRiner, A., Pancost, M.R., Patnaik, A., Shao, W., Shultz, M., Tichkule, R., Tommasi, R.A., Vash, B., Wang, P., Stams, T., 2011. Human HDAC isoform selectivity achieved via exploitation of the acetate release channel with structurally unique small molecule inhibitors. *Bioorganic & Medicinal Chemistry* 19, 4626–4634. <https://doi.org/10.1016/j.bmc.2011.06.030>
16. Galletti, P., Quintavalla, A., Ventrici, C., Giannini, G., Cabri, W., Penco, S., Gallo, G., Vincenti, S., Giacomini, D., 2009. Azetidinones as Zinc-Binding Groups to Design Selective HDAC8 Inhibitors. *ChemMedChem* 4, 1991–2001. <https://doi.org/10.1002/cmdc.200900309>
17. Nian, H., Bisson, W.H., Dashwood, W.-M., Pinto, J.T., Dashwood, R.H., 2009. -Keto acid metabolites of organoselenium compounds inhibit histone deacetylase activity in human colon cancer cells. *Carcinogenesis* 30, 1416–1423. <https://doi.org/10.1093/carcin/bgp147>
18. Hu, E., Dul, E., Sung, C.-M., Chen, Z., Kirkpatrick, R., Zhang, G.-F., Johanson, K., Liu, R., Lago, A., Hofmann, G., Macarron, R., De Los Frailes, M., Perez, P., Krawiec, J., Winkler, J., Jaye, M., 2003. Identification of Novel Isoform-Selective Inhibitors within Class I Histone Deacetylases. *J Pharmacol Exp Ther* 307, 720–728. <https://doi.org/10.1124/jpet.103.055541>
19. Kleinschek, A., Meyners, C., Digiorgio, E., Brancolini, C., Meyer-Almes, F.-J., 2016. Potent and Selective Non-hydroxamate Histone Deacetylase 8 Inhibitors. *ChemMedChem* 11, 2598–2606. <https://doi.org/10.1002/cmdc.201600528>
20. Wolff, B., Jansch, N., Sugiarto, W.O., Frühschulz, S., Lang, M., Altintas, R., Oehme, I., Meyer-Almes, F.-J., 2019. Synthesis and structure activity relationship of 1, 3-benzothiazine-2-thiones as selective HDAC8 inhibitors. *European Journal of Medicinal Chemistry* 184, 111756. <https://doi.org/10.1016/j.ejmech.2019.111756>
21. Amin, Sk.A., Adhikari, N., Jha, T., 2018. Structure-activity relationships of HDAC8 inhibitors: Non-hydroxamates as anticancer agents. *Pharmacological Research* 131, 128–142. <https://doi.org/10.1016/j.phrs.2018.03.001>

22. Goracci, L., Deschamps, N., Randazzo, G.M., Petit, C., Dos Santos Passos, C., Carrupt, P.-A., Simões-Pires, C., Nurisso, A., 2016. A Rational Approach for the Identification of Non-Hydroxamate HDAC6-Selective Inhibitors. *Sci Rep* 6, 29086. <https://doi.org/10.1038/srep29086>
23. Buggy, J.J., Sriram B., Susanne M. S., inventors; Pharmacyclics Inc., assignee; 2015. Uses of selective inhibitors of HDAC8 and treatment of inflammatory conditions. US20150038542.
24. Suzuki, T., Ota, Y., Ri, M., Bando, M., Gotoh, A., Itoh, Y., Tsumoto, H., Tatum, P.R., Mizukami, T., Nakagawa, H., Iida, S., Ueda, R., Shirahige, K., Miyata, N., 2012. Rapid Discovery of Highly Potent and Selective Inhibitors of Histone Deacetylase 8 Using Click Chemistry to Generate Candidate Libraries. *J. Med. Chem.* 55, 9562–9575. <https://doi.org/10.1021/jm300837y>
25. Aaron Beaty Beeler, John A. Porco, Jr., Oscar J. Ingham, James E. Bradner, inventors; Trustees of Boston University, assignee; 2015. Selective histone deacetylase 8 inhibitors. US20150352079.
26. Oyelere, A., Berkley G., inventors; 2013. Histone deacetylase (HDAC) inhibitors targeting prostate tumors and method of making and using thereof. US20130289085.
27. Huang, W.-J., Wang, Y.-C., Chao, S.-W., Yang, C.-Y., Chen, L.-C., Lin, M.-H., Hou, W.-C., Chen, M.-Y., Lee, T.-L., Yang, P., Chang, C.-I., 2012. Synthesis and Biological Evaluation of ortho -Aryl N -Hydroxycinnamides as Potent Histone Deacetylase (HDAC) 8 Isoform-Selective Inhibitors. *ChemMedChem* 7, 1815–1824. <https://doi.org/10.1002/cmdc.201200300>
28. Xu W., Zhang Y., Song W., inventors; Shouguang Fukang Pharmaceuticals Ltd., assignee; 2012. Preparative method and use of ZYJ-D08A and its epimers as histone deacetylase inhibitors. WO2012174730.
29. Xu W., Zhang Y., Fang H., inventors; Shandong University, assignee; 2010. Tyrosine derivatives as histone deacetylase inhibitors and using thereof. CN101723896.
30. Zhang, Y., Feng, J., Liu, C., Zhang, L., Jiao, J., Fang, H., Su, L., Zhang, X., Zhang, J., Li, M., Wang, B., Xu, W., 2010. Design, synthesis and preliminary activity assay of 1,2,3,4-tetrahydroisoquinoline-3-carboxylic acid derivatives as novel Histone deacetylases (HDACs) inhibitors. *Bioorganic & Medicinal Chemistry* 18, 1761–1772. <https://doi.org/10.1016/j.bmc.2010.01.060>
31. Zhang, Y., Feng, J., Jia, Y., Wang, X., Zhang, L., Liu, C., Fang, H., Xu, W., 2011. Development of Tetrahydroisoquinoline-Based Hydroxamic Acid Derivatives: Potent Histone Deacetylase Inhibitors with Marked in Vitro and in Vivo Antitumor Activities. *J. Med. Chem.* 54, 2823–2838. <https://doi.org/10.1021/jm101605z>
32. KrennHrubec, K., Marshall, B.L., Hedglin, M., Verdin, E., Ulrich, S.M., 2007. Design and evaluation of ‘Linkerless’ hydroxamic acids as selective HDAC8 inhibitors. *Bioorganic & Medicinal Chemistry Letters* 17, 2874–2878. <https://doi.org/10.1016/j.bmcl.2007.02.064>
33. Qin, H.-T., Li, H.-Q., Liu, F., 2017. Selective histone deacetylase small molecule inhibitors: recent progress and perspectives. *Expert Opinion on Therapeutic Patents* 27, 621–636. <https://doi.org/10.1080/13543776.2017.1276565>
34. Bressi, J.C., Jong, R. de, Wu, Y., Jennings, A.J., Brown, J.W., O’Connell, S., Tari, L.W., Skene, R.J., Vu, P., Navre, M., Cao, X., Gangloff, A.R., 2010. Benzimidazole and imidazole inhibitors of histone deacetylases: Synthesis and biological activity. *Bioorganic*

- & Medicinal Chemistry Letters 20, 3138–3141.
<https://doi.org/10.1016/j.bmcl.2010.03.092>
35. Mohan, R., Sharma, A.K., Gupta, S., Ramaa, C.S., 2012. Design, synthesis, and biological evaluation of novel 2,4-thiazolidinedione derivatives as histone deacetylase inhibitors targeting liver cancer cell line. *Med Chem Res* 21, 1156–1165. <https://doi.org/10.1007/s00044-011-9623-3>
36. Marek, M., Shaik, T.B., Heimburg, T., Chakrabarti, A., Lancelot, J., Ramos-Morales, E., Da Veiga, C., Kalinin, D., Melesina, J., Robaa, D., Schmidtkunz, K., Suzuki, T., Holl, R., Ennifar, E., Pierce, R.J., Jung, M., Sippl, W., Romier, C., 2018. Characterization of Histone Deacetylase 8 (HDAC8) Selective Inhibition Reveals Specific Active Site Structural and Functional Determinants. *J. Med. Chem.* 61, 10000–10016. <https://doi.org/10.1021/acs.jmedchem.8b01087>
37. Hou, X., Du, J., Liu, R., Zhou, Y., Li, M., Xu, W., Fang, H., 2015. Enhancing the Sensitivity of Pharmacophore-Based Virtual Screening by Incorporating Customized ZBG Features: A Case Study Using Histone Deacetylase 8. *J. Chem. Inf. Model.* 55, 861–871. <https://doi.org/10.1021/ci500762z>
38. Patil, V., Tilekar, K., Mehendale-Munj, S., Mohan, R., Ramaa, C.S., 2010. Synthesis and primary cytotoxicity evaluation of new 5-benzylidene-2,4-thiazolidinedione derivatives. *European Journal of Medicinal Chemistry* 45, 4539–4544. <https://doi.org/10.1016/j.ejmech.2010.07.014>
39. Kabir, A., Tilekar, K., Upadhyay, N., Ramaa, C.S., 2019. Novel Anthraquinone Derivatives as Dual Inhibitors of Topoisomerase 2 and Casein Kinase 2: In Silico Studies, Synthesis and Biological Evaluation on Leukemic Cell Lines. *ACAMC* 18, 1551–1562. <https://doi.org/10.2174/1871520618666180423111309>
40. Momose, Y., Meguro, K., Ikeda, H., Hatanaka, C., Oi, S., Sohda, T., 1991. Studies on Antidiabetic Agents. X. Synthesis and Biological Activities of Pioglitazone and Related Compounds. *Chem. Pharm. Bull.* 39, 1440–1445. <https://doi.org/10.1248/cpb.39.1440>
41. Auld, D.S., Thorne, N., Maguire, W.F., Inglese, J., 2009. Mechanism of PTC124 activity in cell-based luciferase assays of nonsense codon suppression. *Proceedings of the National Academy of Sciences* 106, 3585–3590. <https://doi.org/10.1073/pnas.0813345106>
42. Schmidt, C., 2010. GSK/Sirtris compounds dogged by assay artifacts. *Nat Biotechnol* 28, 185–186. <https://doi.org/10.1038/nbt0310-185>
43. Guha, M., 2011. PARP inhibitors stumble in breast cancer. *Nat Biotechnol* 29, 373–374. <https://doi.org/10.1038/nbt0511-373>
44. Liu, X., Shi, Y., Maag, D.X., Palma, J.P., Patterson, M.J., Ellis, P.A., Surber, B.W., Ready, D.B., Soni, N.B., Ladrer, U.S., Xu, A.J., Iyer, R., Harlan, J.E., Solomon, L.R., Donawho, C.K., Penning, T.D., Johnson, E.F., Shoemaker, A.R., 2012. Iniparib Nonselectively Modifies Cysteine-Containing Proteins in Tumor Cells and Is Not a Bona Fide PARP Inhibitor. *Clinical Cancer Research* 18, 510–523. <https://doi.org/10.1158/1078-0432.CCR-11-1973>
45. Florio, M., Borrell, V., Huttner, W.B., 2017. Human-specific genomic signatures of neocortical expansion. *Current Opinion in Neurobiology* 42, 33–44. <https://doi.org/10.1016/j.conb.2016.11.004>
46. Florio, M., Heide, M., Pinson, A., Brandl, H., Albert, M., Winkler, S., Wimberger, P., Huttner, W.B., Hiller, M., 2018. Evolution and cell-type specificity of human-specific

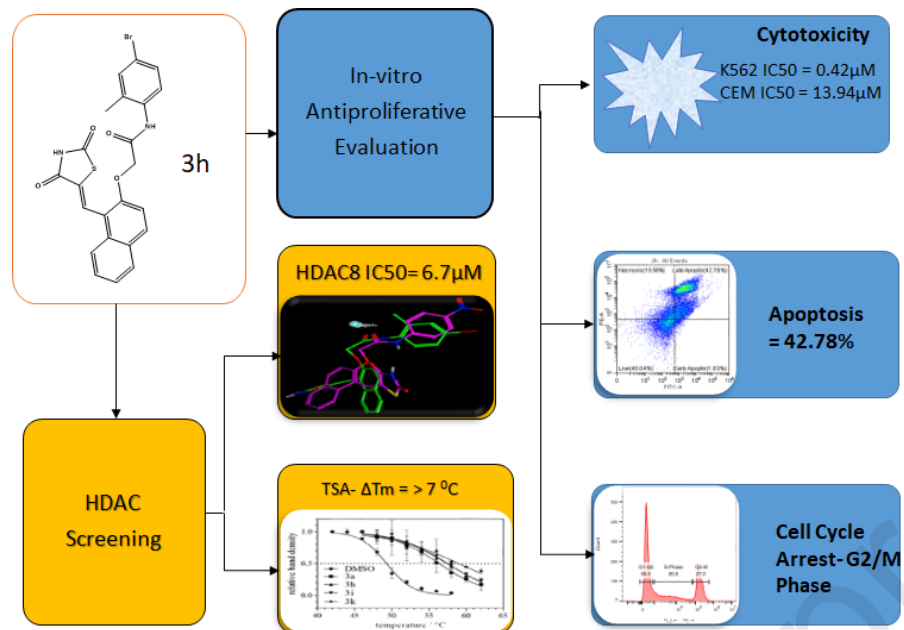
- genes preferentially expressed in progenitors of fetal neocortex. *eLife* 7, e32332. <https://doi.org/10.7554/eLife.32332>
47. Song, S., Wang, Y., Xu, P., Yang, R., Ma, Z., Liang, S., Zhang, G., 2015. The inhibition of histone deacetylase 8 suppresses proliferation and inhibits apoptosis in gastric adenocarcinoma. *International Journal of Oncology* 47, 1819–1828. <https://doi.org/10.3892/ijo.2015.3182>
48. Wu, J., Du, C., Lv, Z., Ding, C., Cheng, J., Xie, H., Zhou, L., Zheng, S., 2013. The Up-Regulation of Histone Deacetylase 8 Promotes Proliferation and Inhibits Apoptosis in Hepatocellular Carcinoma. *Dig Dis Sci* 58, 3545–3553. <https://doi.org/10.1007/s10620-013-2867-7>
49. Paris, M., Porcelloni, M., Binaschi, M., Fattori, D., 2008. Histone Deacetylase Inhibitors: From Bench to Clinic. *J. Med. Chem.* 51, 1505–1529. <https://doi.org/10.1021/jm7011408>
50. Dong, Z., Yang, Y., Liu, S., Lu, J., Huang, B., Zhang, Y., 2018. HDAC inhibitor PAC-320 induces G2/M cell cycle arrest and apoptosis in human prostate cancer. *Oncotarget* 9. <https://doi.org/10.18632/oncotarget.23070>
51. Vannini, A., Volpari, C., Filocamo, G., Casavola, E.C., Brunetti, M., Renzoni, D., Chakravarty, P., Paolini, C., De Francesco, R., Gallinari, P., Steinkuhler, C., Di Marco, S., 2004. Crystal structure of a eukaryotic zinc-dependent histone deacetylase, human HDAC8, complexed with a hydroxamic acid inhibitor. *Proceedings of the National Academy of Sciences* 101, 15064–15069. <https://doi.org/10.1073/pnas.0404603101>
52. Decroos, C., Clausen, D.J., Haines, B.E., Wiest, O., Williams, R.M., Christianson, D.W., 2015. Variable Active Site Loop Conformations Accommodate the Binding of Macrocyclic Largazole Analogues to HDAC8. *Biochemistry* 54, 2126–2135. <https://doi.org/10.1021/acs.biochem.5b00010>
53. Somoza, J.R., Skene, R.J., Katz, B.A., Mol, C., Ho, J.D., Jennings, A.J., Luong, C., Arvai, A., Buggy, J.J., Chi, E., Tang, J., Sang, B.-C., Verner, E., Wynands, R., Leahy, E.M., Dougan, D.R., Snell, G., Navre, M., Knuth, M.W., Swanson, R.V., McRee, D.E., Tari, L.W., 2004. Structural Snapshots of Human HDAC8 Provide Insights into the Class I Histone Deacetylases. *Structure* 12, 1325–1334. <https://doi.org/10.1016/j.str.2004.04.012>
54. Deschamps, N., Simões-Pires, C.A., Carrupt, P.-A., Nurisso, A., 2015. How the flexibility of human histone deacetylases influences ligand binding: an overview. *Drug Discovery Today* 20, 736–742. <https://doi.org/10.1016/j.drudis.2015.01.004>
55. Daina, A., Michielin, O., Zoete, V., 2017. SwissADME: a free web tool to evaluate pharmacokinetics, drug-likeness and medicinal chemistry friendliness of small molecules. *Sci Rep* 7, 42717. <https://doi.org/10.1038/srep42717>
56. Jänsch, N., Meyners, C., Muth, M., Koprancovic, A., Witt, O., Oehme, I., Meyer-Almes, F.-J., 2019. The enzyme activity of histone deacetylase 8 is modulated by a redox-switch. *Redox Biology* 20, 60–67. <https://doi.org/10.1016/j.redox.2018.09.013>
57. Volund, A., 1978. Application of the Four-Parameter Logistic Model to Bioassay: Comparison with Slope Ratio and Parallel Line Models. *Biometrics* 34, 357. <https://doi.org/10.2307/2530598>
58. Schweipert, M., Jänsch, N., Sugiarto, W.O., Meyer-Almes, F.-J., 2019. Kinetically selective and potent inhibitors of HDAC8. *Biological Chemistry* 400, 733–743. <https://doi.org/10.1515/hsz-2018-0363>

59. Bhat, S.S., Revankar, V.K., Kumbar, V., Bhat, K., Kawade, V.A., 2018. Synthesis, crystal structure and biological properties of a cis -dichloridobis(diimine)copper(II) complex. *Acta Crystallogr C Struct Chem* 74, 146–151. <https://doi.org/10.1107/S2053229617018551>
60. Peram, M.R., Jalalpure, S., Kumbar, V., Patil, S., Joshi, S., Bhat, K., Diwan, P., 2019. Factorial design based curcumin ethosomal nanocarriers for the skin cancer delivery: in vitro evaluation. *Journal of Liposome Research* 29, 291–311. <https://doi.org/10.1080/08982104.2018.1556292>

Highlights:

- Selective and Non-hydroxamate HDAC8 inhibitors instead pan inhibitors.
- 5-Naphthylidene-2,4-thiazolidinedione derivatives were designed and synthesized.
- Most potent compound 3k showed HDAC8 inhibition with IC₅₀ of 2.7μM.
- Antiproliferative effects- HDAC8 inhibition, Apoptosis and Cell cycle arrest.
- Docking found to be consistent with experimental activity in terms of IC₅₀-values

GA



Declaration of interests

The authors declare that they have no known competing financial interests or personal relationships that could have appeared to influence the work reported in this paper.

The authors declare the following financial interests/personal relationships which may be considered as potential competing interests:

Journal Pre-proofs